Genetically encoded ratiometric biosensor for probing lysosomal pH in mammalian cells and *C. elegans*

Marcus Y. Chin[1,2*], Anand R. Patwardhan[1*], Kean-Hooi Ang[2], Austin L. Wang[1], Carolina Alquezar[1], Mackenzie Welch[1], Michael Grabe[3], Michelle R. Arkin[2†] and Aimee W. Kao[1†]

[1]Memory and Aging Center, Department of Neurology, University of California, San Francisco, California, CA 94158, USA

[2]Small Molecule Discovery Center, Department of Pharmaceutical Chemistry, University of California, San Francisco, CA 94143, USA

[3]Department of Pharmaceutical Chemistry and Cardiovascular Research Institute, University of California, San Francisco, CA 94158, USA

[*] Both authors contributed equally to this manuscript

[†] Corresponding authors: aimee.kao@ucsf.edu and michelle.arkin@ucsf.edu

Key words: pH sensor, lysosomes, ratiometric imaging, neurons, *C. elegans*

Abbreviations: *FIRE-pHLy, Fluorescence Indicator REporting pH in Lysosomes; LAMP1, Lysosomal-associated membrane protein 1; LAMP2, Lysosomal-associated membrane protein 2; V-ATPase, Vacuolar-type ATPase; FP, Fluorescent Protein; mTFP1, monomeric teal fluorescent protein; DAMP, (N-(3-((2,4-dinitrophenyl)amino)propyl)-N-(3-aminopropyl)methylamine, dihydrochloride; FITC; fluorescein isothiocyanate; BafA1, Bafilomycin A1; iPSC, Induced pluripotent stem cells; HEK293, human embryonic kidney 293; RA, Retinoic acid; BDNF, Brain-derived neurotrophic factor; CMV, cytomegalovirus; UbC, ubiquitin C.*

ABSTRACT

Lysosomes are important sites for macromolecular degradation, defined by a profoundly acidic lumenal pH of ~4.5. To better understand lysosomal pH, we designed a novel, genetically encoded, fluorescent protein-based pH biosensor called FIRE-pHLy (Fluorescence Indicator REporting pH in Lysosomes). This sensor was targeted to lysosomes with LAMP1 and reported lumenal pH between 3.0 and 6.0 with monomeric teal fluorescent protein 1 (mTFP1), a bright cyan FP variant with a pKa of 4.3. Ratiometric quantification was enabled with cytosolically oriented mCherry using high-content imaging. We expressed FIRE-pHLy in several cellular models as well as the multicellular organism *C. elegans* and quantified its alkalinizing response to bafilomycin A1, a specific V-ATPase inhibitor. In summary, we have engineered FIRE-pHLy, a specific, robust and versatile lysosomal pH biosensor that has broad applications for investigating pH dynamics in aging and lysosome-related diseases, as well as in lysosome-based drug discovery.

INTRODUCTION

Lysosomes support diverse cellular functions by acting as sites of macromolecular degradation, nutrient recycling, pathogen clearance and signaling events that regulate cellular functions (Huynh et al., 2007; Lawrence & Zoncu, 2019; Mony et al., 2016; Settembre et al., 2013). Mammalian cells eliminate misfolded proteins using either the ubiquitin-proteasome system or autophagy-lysosome pathway. Both play indispensable roles in protein quantity and quality control in the cell (Ballabio & Bonifacino, 2020; Rousseau & Bertolotti, 2018). The degradative abilities of lysosomes are conferred by an extremely acidic lumen (pH ~4.5-4.7) (Casey et al., 2010) which contains more than fifty hydrolytic enzymes, also known as "acid hydrolases" that break down major macromolecules into building blocks that are recycled for cellular reuse (de Duve & Wattiaux, 1966; Ishida et al., 2013; Rudnick, 1987). Lysosomal acidity is maintained through the vacuolar-type H^+-ATPase (V-ATPase) proton pump, an evolutionarily conserved electrogenic pump that generates a proton gradient across membranes through coupling proton translocation with ATP hydrolysis (Beyenbach & Wieczorek, 2006). Additional contributions to lysosomal pH setpoint are made by a number of counter ion channels and transporters (Mindell, 2012).

Lysosomal pH dynamics are broadly implicated in biological and disease pathways. Loss-of-function mammalian V-ATPase mutations are embryonic lethal (Inoue et al., 1999), highlighting the significance of lysosomal function, in particular pH, to the sustainment of life. In cancer, aberrant V-ATPase activity is linked to hyper-acidic lysosomes that promote tumor proliferation and invasion (Kallunki et al., 2013; Liu et al., 2018; Webb et al., 2011). Even relatively small alterations in the proton concentration (~0.5 – 0.9 pH units) can have dramatic effects on tumor aggressiveness (Anderson et al., 2016; Gallagher et al., 2008). In contrast, loss of lysosomal acidity is observed in aging. Yeast vacuoles (metazoan homolog of lysosomes) and *C. elegans* lysosomes lose their acidity with increasing age (Baxi et al., 2017; Hughes & Gottschling, 2012; Sun et al., 2020), but can be rescued with caloric restriction that upregulates V-ATPase activity (Hughes & Gottschling, 2012). Additionally, neuronal health is highly regulated by lysosomal function, as demonstrated by insights from human genetics that link lysosomal dysfunction to a wide range of neurological diseases (Malik et al., 2019; Platt et al., 2012). Notably, reduced lysosomal pH is a probable key factor in the pathogenesis of familial forms of Alzheimer's disease, Parkinson's disease, prion diseases and amyotrophic lateral

75 sclerosis (Bourdenx et al., 2016; Coffey et al., 2014; Van Acker et al., 2019; Wolfe et al., 2013).
76 Furthermore, Alzheimer's disease-related presenilin-1 mutations have been shown to prevent
77 proper acidification of lysosomes by inhibiting assembly of V-ATPase subunits (Fang et al.,
78 2010; Lee et al., 2015; Wolfe et al., 2013). These studies highlight the importance of
79 investigating lysosomal pH regulatory mechanisms as a potential therapeutic target.

80 Several small-molecule pH-sensitive dyes, organic fluorophores and synthetic probes
81 (e.g. LysoSensor, Lysotracker, FITC-dextran, pHrodo-dextran, DAMP, quantum dots) label and
82 measure lysosomal pH within cells (Han & Burgess, 2010; Jin et al., 2010; Ohkuma, 1989; X.
83 Wang et al., 2020; Wolfe et al., 2013; X.-X. Zhang et al., 2013). However, these probes have
84 disadvantages due to their poor specificity of subcellular targeting, cytotoxicity, modification of
85 cellular metabolic activity, and leakage from cells (Han & Burgess, 2010; Pierzyńska-Mach et
86 al., 2014; Tantama et al., 2011). The first genetically encoded intracellular pH sensors (called
87 'pHluorins') were developed through directed mutations of specific residues of green fluorescent
88 protein (GFP) to pH-sensitive histidine residues (Miesenböck et al., 1998). Subsequent variants
89 of this biosensor were targeted towards a cytosolic pH range (6.8 to 7.2) (Casey et al., 2010) and
90 have been reviewed elsewhere (Ashby et al., 2004; Benčina, 2013). Genetically encoded pH
91 biosensors have many advantages such as (i) controlled expression in different cell types and
92 tissues, (ii) enhanced intracellular specificity and (iii) bypassing of dye-incubation steps to (iv)
93 enable long-term, live imaging studies in cells and animals. Despite these advantages, currently
94 there are only a very limited number of biosensors suitable for reporting the acidic pH range of
95 lysosomes.

96 Using the diverse toolkit of FPs (Lambert, 2019; Rodriguez et al., 2017), we engineered a
97 novel lysosomally targeted cyan and red fusion protein to report lysosomal pH. We call this
98 fusion protein Fluorescence Indicator REporting pH in Lysosomes, or 'FIRE-pHLy'. FIRE-
99 pHLy showed specificity with respect to lysosomal localization and for sensing protons within a
100 dynamic pH range of 3.0 - 6.0. Further, when exposed to bafilomycin A1, a known V-ATPase
101 inhibitor that alkalinizes lysosomes, FIRE-pHLy demonstrated a dynamic pH response in a
102 variety of cell types. Unbiased high-content imaging of FIRE-pHLy allowed us to reproducibly
103 quantify these responses. Given the emerging attention to lysosomal pH in neurodegeneration
104 and aging, we explored the utility of FIRE-pHLy in the context of primary neurons, human
105 induced pluripotent stem cells (iPSCs), neuroblastoma cells and the model organism *C. elegans.*

106 Thus, FIRE-pHLy represents a novel lysosomal pH sensor with multiple applications, including
107 the possibility of future use in elucidating pH dynamics in aging and other lysosome-related
108 diseases.

RESULTS

Design principles for a ratiometric lysosomal pH sensor

To develop a reliable lysosomal pH biosensor that can be applied to any cellular or *in vivo* model, we have selected a ratiometric system in which the relative brightness of two reporters is used to quantify pH measurements. In a dual-reporter, ratiometric system, one fluorophore changes its signal in response to proton concentration while the other serves as a stable reference point for identifying lysosomes and normalizing protein expression, degradation and photobleaching. This capability represents a significant advantage over single fluorophore biosensors that can lead to biased measurements between samples or experiments (Grillo-Hill et al., 2014; O'Connor & Silver, 2013).

For our purposes, a ratiometric lysosomal pH reporter required the following features: 1) a domain for lysosomal targeting, 2) a cytosolically facing fluorescent protein that exhibits stable brightness at physiological intracellular pH (range pH 6.8 to 7.2) (Casey et al., 2010) and 3) a lysosomal lumen-facing fluorescent protein that provides dynamic lysosomal pH sensing at highly acidic pH (pH <5.0). For lysosomal targeting, we utilized LAMP1, a type 1 membrane protein harboring a tyrosine-based lysosomal sorting motif in its short cytoplasmic tail (last 5 amino acids 'GYQTI') (Braulke & Bonifacino, 2009; Rohrer et al., 1996). For the cytosolic, pH-insensitive domain of the reporter, we tested a number of candidates and ultimately chose mCherry for its brightness and fluorescent stability at physiological intracellular pH ranges (Mony et al., 2016).

The success of a lysosomal pH sensor depends upon identifying a fluorescent protein that accurately reflects the highly acidic pH of the lysosome. The ideal fluorescent protein for this purpose requires a low pKa to allow for pH sensing within the anticipated lysosomal pH range. Additional major attributes in choosing a pH-sensitive fluorescent protein include high brightness, photostability and the ability to maintain proper protein folding and integrity within the acidic lysosomal environment. After testing different candidates, we selected mTFP1 (monomeric teal fluorescent protein 1), a variant of cyan fluorescent protein with a pKa of 4.3. mTFP1 possesses a robust sigmoidal pH response *in vitro* across a broad range (pH 2.0 – 9.0) (Ai et al., 2006). It also exhibits a high extinction coefficient (64000 units) with a brightness value of 54 units and demonstrates adequate photostability ($t_{1/2}$ = 163.0 s) (Ai et al., 2006;

139 Cranfill et al., 2016; Shaner et al., 2004). Thus, mTFP1 offers the optimal balance of favorable
140 attributes for the pH-sensitive aspect of a ratiometric pH sensor.

141 The assembled chimeric fluorescent protein construct consisted of an N-terminal,
142 lysosomal lumen-facing, pH-sensitive mTFP1 fused to the transmembrane portion of human
143 LAMP1 and a C-terminal, lysosomal pH-insensitive mCherry (**Fig. 1A, B**). A flexible linker
144 (GGSGGGSGSGGGSG), rich in small and polar amino acids, was added between mTFP1 and
145 LAMP1 to promote correct protein folding and retention of biological and fluorescence
146 properties (Chen et al., 2013). To allow correct sorting, maintain a fixed distance between the
147 two proteins and minimize mCherry aggregation, a rigid linker (PAPAPAP) was placed between
148 LAMP1 and mCherry (Chen et al., 2013; Shemiakina et al., 2012). Expression of the construct
149 was driven by the human cytomegalovirus (CMV) promoter.

150 Spectral compatibility is important in dual-color, ratiometric reporters. To assess for this
151 in our reporter, we verified the *in vitro* excitation and emission wavelengths for mTFP1 (462 and
152 492 nm, respectively) and mCherry (587 and 610 nm, respectively) (Ai et al., 2006; Shcherbo et
153 al., 2007). We excited mTFP1 using a 470 nm laser line and detected emission from 475 to 580
154 nm. For mCherry, we excited at 587 nm and detected from 592 to 779 nm. Given their distinct
155 spectral properties, mTFP1 and mCherry exhibited ideal spectral compatibility (**Fig. 1C**).

156 Using lentiviral transduction, our pH sensor was stably expressed in cell lines such as
157 human embryonic kidney 293 (HEK293FT) cells and imaged using the abovementioned
158 conditions (**Fig. 1D)**. Finally, we probed lysates of cells expressing FIRE-pHLy via western
159 blotting with human anti-LAMP1 antibody and confirmed expression **(Fig. 1E)**. We designated
160 the resulting chimeric fluorescent protein as FIRE-pHLy, for Fluorescence Indicator REporting
161 pH in Lysosomes.
162
163
164
165
166
167
168
169
170
171

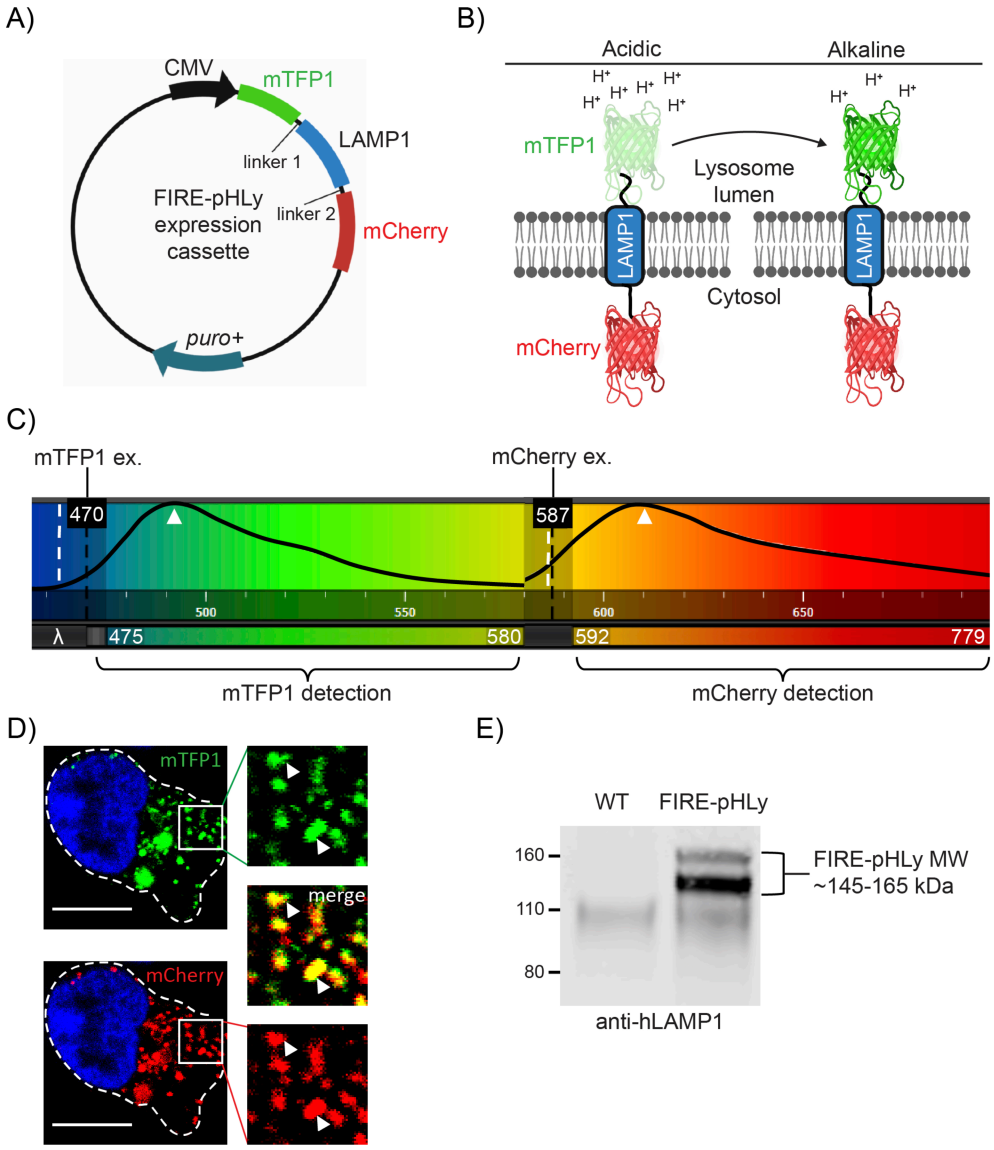

Figure 1. Design of ratiometric lysosomal pH sensor - FIRE-pHLy

(A) Design of FIRE-pHLy expression cassette driven by CMV promoter cloned in the lentiviral pJLM puromycin-resistant plasmid. Chimeric protein (N- to C-terminus) mTFP1-LAMP1-mCherry is targeted to lysosomes via the type-I transmembrane human LAMP1 peptide sequence. Linker regions 1 (GGSGGGSGSGGGSG) and 2 (PAPAPAP) allow proper folding and expression of each protein portion. **(B)** Representation of FIRE-pHLy expressed on lysosomal membranes and mTFP1 fluorescence levels in acidic (low pH) and alkaline (high pH) conditions. Lysosomal pH-sensitive mTFP1 located within the lumen and lysosomal pH-insensitive mCherry is located on the cytosolic side. **(C)** Laser excitation (black dashed lines) and detection wavelengths (nm) used to image mTFP1 and mCherry fluorescence. As reported in literature, white dashed lines indicate expected peak excitation (mTFP1 = 462 nm; mCherry = 587 nm) while arrowheads indicate expected peak emission (mTFP1 = 492 nm; mCherry 610 nm). **(D)** Representative confocal fluorescence images of mTFP1 (green), mCherry (red) and merged (yellow) in stable FIRE-pHLy-expressing HEK293FT cells. Arrowheads highlight representative puncta of

overlapping mTFP1 and mCherry signal. Scale bar = 10 µm. (**E**) Lysates from wild-type (WT) and FIRE-pHLy-expressing HEK293FT cells were western blotted with anti-hLAMP1 antibody to detect intact FIRE-pHLy fusion protein expression levels. The expected FIRE-pHLy molecular weight (MW) is between 145-165 kDa, depending on the glycosylation state of LAMP1 (~90-110 kDa). The MW of mTFP1 and mCherry are 26 and 29 kDa, respectively.

FIRE-pHLy specifically localized to lysosomal compartments

We first investigated whether FIRE-pHLy sorted to bona fide lysosomal compartments in HEK293FT cells stably expressing the reporter. To do so, we tested colocalization of FIRE-pHLy with lysosomal, endosomal and mitochondrial sub-cellular markers (**Fig. 2A-E**). Cells were imaged using immunofluorescence confocal microscopy with three laser channels. As expected, since they are co-expressed in the same fusion protein, mTFP1 and mCherry showed consistently strong positive Pearson's correlation coefficient values (within the range r = 0.78 – 0.82) across all images (**Fig. 2F-J**).

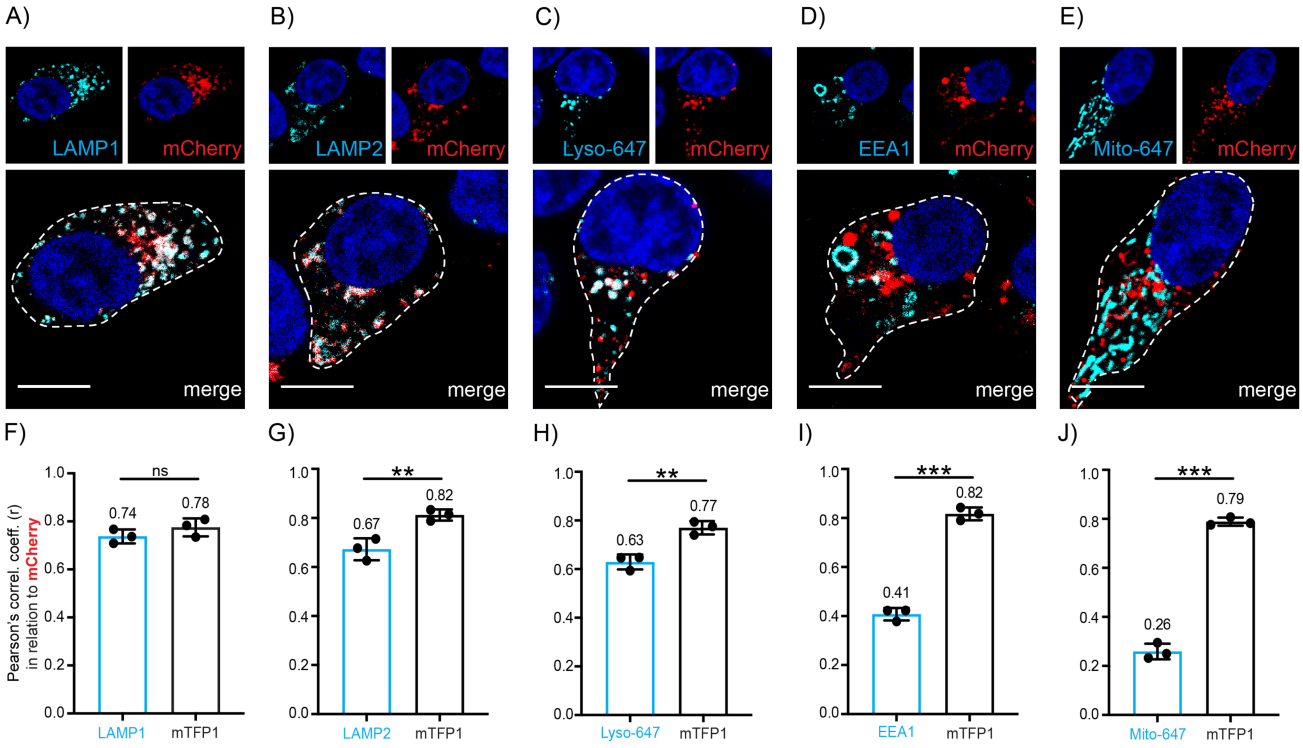

Figure 2. FIRE-pHLy localizes to lysosomal compartments

(A-E) Representative images of FIRE-pHLy-expressing HEK293FT cells stained with various markers (shown in light blue). **(A)** LAMP1 (lysosomal membranes), **(B)** LAMP2 (lysosomal membranes), **(C)** LysoTracker Deep Red or Lyso-647 (acidic compartments), **(D)** EEA1 (early endosomes), **(E)** MitoTracker Deep Red or Mito-647

228 (mitochondria). Scale bar = 10 μm. Co-localized marker and mCherry puncta in displayed in white. Nuclei are
229 shown in dark blue. **(F-J)** Displayed below each image set are Pearson's correlation coefficients (r) calculated using
230 the ImageJ plugin JACoP (Just Another Colocalization Plugin). Each graph shows a different marker colocalized
231 with mCherry and mTFP1 colocalized with mCherry. Data points represents mean ± S.D. (3 independent replicates;
232 n = 15 cells/replicate. Statistical analysis was performed using two-tailed, unpaired Student's *t*-test. *p ≤ 0.05; **p ≤
233 0.01; ***p ≤ 0.001; ns = not significant).
234
235 We then quantified the colocalization of FIRE-pHLy (using mCherry as reference) with
236 existing markers for various sub-cellular organelles. We first assessed lysosomal markers by
237 immunostaining for endogenous LAMP1 or LAMP2 or using lysotracker 647. LAMP1 and
238 LAMP2 are among the most abundant lysosome-associated membrane proteins (Eskelinen,
239 2006; Saftig & Klumperman, 2009). Endogenous LAMP1 and mCherry showed a very strong
240 positive correlation (r = 0.74 ± 0.03) (**Fig. 2A**). Similarly, LAMP2, a well characterized regulator
241 of autophagy (Tekirdag & Cuervo, 2018), colocalized with mCherry (r = 0.67 ± 0.04) (**Fig. 2B**).
242 LysoTracker Deep Red (Lyso-647) is a widely used commercially available fluorescent probe
243 that preferentially accumulates in acidic vesicular compartments, such as late endosomes and
244 lysosomes (Chazotte, 2011). Co-localization of Lyso-647 and mCherry was moderately strong (r
245 = 0.63 ± 0.03) (**Fig. 2C**). On the contrary, early endosome antigen 1 (EEA1) is a membrane-
246 bound protein found specifically on early endosomes (Mu et al., 1995) and its labeling is
247 characterized by large distinct ring-like structures (Wilson et al., 2000). In contrast to the
248 lysosomal markers, only a lower fraction of mCherry associated with EEA1 (r = 0.41 ± 0.02)
249 (**Fig. 2D**) likely reflecting the maturation of lysosomes from the highly dynamic endolysomal
250 continuum (Jovic et al., 2010).
251 Finally, MitoTracker Deep Red (Mito-647) was used to stain mitochondria as a negative
252 control (**Fig. 2E**). Most Mito-647 did not strongly colocalize with FIRE-pHLy (r = 0.26 ± 0.03).
253 The small percentage of colocalization was anticipated because mitochondria-lysosome crosstalk
254 is known to occur (Deus et al., 2020; Lahuerta et al., 2018). Taken together, we concluded that
255 FIRE-pHLy localization exhibited normal trafficking and sorting pathways with high specificity
256 towards lysosomal membranes as defined by its LAMP1 and LAMP2 colocalization.
257 **Quantification & visualization of pH-dependent, mTFP1 fluorescence in live cells**
258 Next, we characterized the ability of FIRE-pHLy to report lysosomal pH in living cells.
259 To do so, we first established a robust quantitative high-content analysis workflow to acquire

260 ratiometric confocal images (**Fig. 3A**). Automated, multi-wavelength imaging represents a
261 powerful technical advance that allows rapid acquisition of unbiased, large-scale, cell population
262 images while minimizing the potential variation of manual imaging. Furthermore, high-content
263 image analysis techniques enable nested post-processing features that precisely quantify cellular
264 phenotypes of interest while removing background noise.

265 Here, we built a specific lysosomal segmentation protocol that extracted relevant image
266 information, such as fluorescence intensities and nucleus count, to assess pH dependence in
267 FIRE-pHLy-expressing cells (See Methods for details). After seeding HEK293FT cells stably
268 expressing FIRE-pHLy into 96-well microplates, we examined proton (H^+)-dependent mTFP1
269 fluorescence by artificially adjusting lysosomal pH using ionophores. Prior to imaging, the cell
270 culture media was exchanged with pH calibration buffers (pH 2.0 to 7.0) supplemented with 10
271 μM nigericin (Wolfe et al., 2013) and 1X monensin to permeabilize membranes. Nigericin
272 (K^+/H^+) and monensin (Na^+/H^+) are well-characterized ionophores that exchange K^+ (and to a
273 lesser extent Na^+) for H^+ across cell membranes, thus equilibrating external pH with that of the
274 lysosomal lumen (Harned et al., 1951; Wolfe et al., 2013). After 10 minutes of incubation,
275 simultaneous dual color live confocal images were rapidly acquired with an automated confocal
276 microscope to obtain accurate fluorescence values for mTFP1 and mCherry across different pH
277 values.

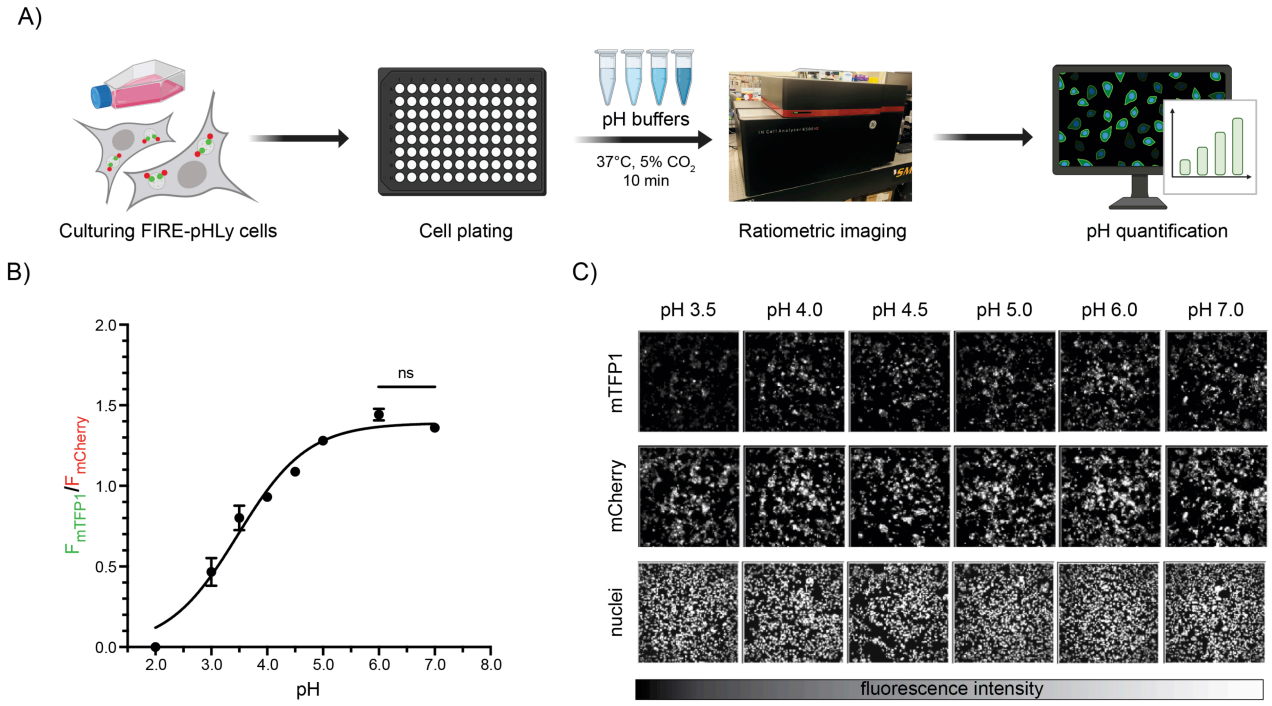

Figure 3. pH calibration in live FIRE-pHLy-expressing HEK293FT cells

(A) High-throughput workflow for pH calibration protocol. FIRE-pHLy-expressing HEK293FT cells were seeded in 96-well assay plates, incubated with pH buffers (adjusted to 2.0, 3.0, 3.5, 4.0, 4.5, 5.0, 6.0 and 7.0), imaged live using a high-content confocal image analyzer and quantified. **(B)** Fluorescence ratios ($F_{mTFP1}/F_{mCherry}$) were plotted against pH values to generate a sigmoidal pH calibration curve. Data points are presented as mean ± S.D., from 4 independent replicates; n=10,000 cells per replicate. Curve was fitted using a sigmoidal nonlinear regression model with the x-axis constrained at 0. Tukey's test for multiple stepwise comparisons indicated significance between all pH groups, except pH 6.0 and pH 7.0. **(C)** Black and white images of mTFP1, mCherry and nuclei taken from one field of one representative assay well from different pH conditions.

To quantify lysosomal pH, fluorescence intensity ratios for mTFP1 and mCherry ($F_{mTFP1}/F_{mCherry}$) were calculated and plotted according to the pH of the buffer. Measurements were then fitted to generate a pH calibration curve **(Fig. 3B).** The ratio curve exhibited a significant positive sigmoidal relationship with pH, showing a two-fold change in fluorescence ratio between pH 3.0 and 6.0.

As anticipated, mTFP1 fluorescence was the sole driver of the FIRE-pHLy ratio change. mTFP1 signal decreased under acidic conditions, with fluorescence quenching below pH 3.5. mTFP1 exhibited increasing brightness in less acidic buffer conditions of pH 5.0 to 6.0 with plateauing of fluorescence above pH 6.0 **(Fig. 3C).** In accordance with its reported pKa of ~4.3, mTFP1 reproducibly measured pH within the ionophore induced pH range 3.0 to 6.0, making it

298 one of the most robust fluorophores for engineering a genetically encoded lysosomal pH sensor
299 to date. The fluorescence of mCherry remained stable over a considerable range of pH values
300 (see Discussion) and Hoechst nuclear staining also provided a pH-independent cell count.
301 Collectively, these results confirmed FIRE-pHLy as a robust, highly quantitative, non-invasive
302 tool to measure lysosomal pH in live cells using high-content microscopy.
303
304 **Functional validation of FIRE-pHLy in different cell types**
305 Optimal lysosomal pH is maintained by the V-ATPase proton pump, a multi-subunit
306 protein complex localized on lysosomal membranes that generates an inward proton flux to
307 acidify lysosomes (Mindell, 2012). Bafilomycin A1 (BafA1) is a potent V-ATPase inhibitor and
308 functions by binding to the V0c subunit, thus blocking proton translocation (Dröse & Altendorf,
309 1996). To further validate FIRE-pHLy in fixed cells **(Fig. 4A)**, pH was measured after
310 alkalinizing lysosomes using BafA1. FIRE-pHLy-expressing HEK293FT cells were incubated
311 with pH buffers similar to methods described above, fixed, and imaged to generate a standard pH
312 calibration curve **(Fig. 4B)**. Cells were treated with BafA1 concentrations of 30 nM to 1000 nM
313 **(Fig 4C)**. Lysosomal pH increased dose-dependently with BafA1 concentration, plateauing at
314 300 nM with a pH~5.6 compared to the control-treatment group pH of ~4.1.
315 Given that FIRE-pHLy behaved as a robust ratiometric pH biosensor, we sought to
316 functionally validate its utility in a variety of different cell types. First, we performed lentiviral
317 transduction to generate stable FIRE-pHLy lines in induced pluripotent stem cells (iPSCs), SH-
318 SY5Y neuroblastoma cells, retinoic acid-differentiated SH-SY5Y neuron-like cells and primary
319 rat neurons **(Fig. 4D-G)**. For transduction into iPSCs, the CMV promoter was exchanged for a
320 human ubiquitin C (UbC) promoter-driven lentiviral FIRE-pHLy construct, since CMV is
321 silenced by DNA methylation during differentiation and shows weak activity in certain cell types
322 including iPSCs (Brooks et al., 2004; Meilinger et al., 2009). FIRE-pHLy-expressing stable cell
323 lines were treated with 100nM BafA1 for 6 hours, a condition that we previously determined to
324 reliably induce pH elevation (pH~5.1). Cells were then fixed and subjected to high content
325 imaging and analysis. Elevation of lysosomal pH would be expected to increase mTFP1
326 fluorescence, thus increasing the FIRE-pHLy fluorescence ratio. Indeed, comparisons of ratios
327 with and without BafA1 treatment confirmed that FIRE-pHLy detected lysosomal alkalization
328 across all cell lines tested (**Fig. 4H-K)**.

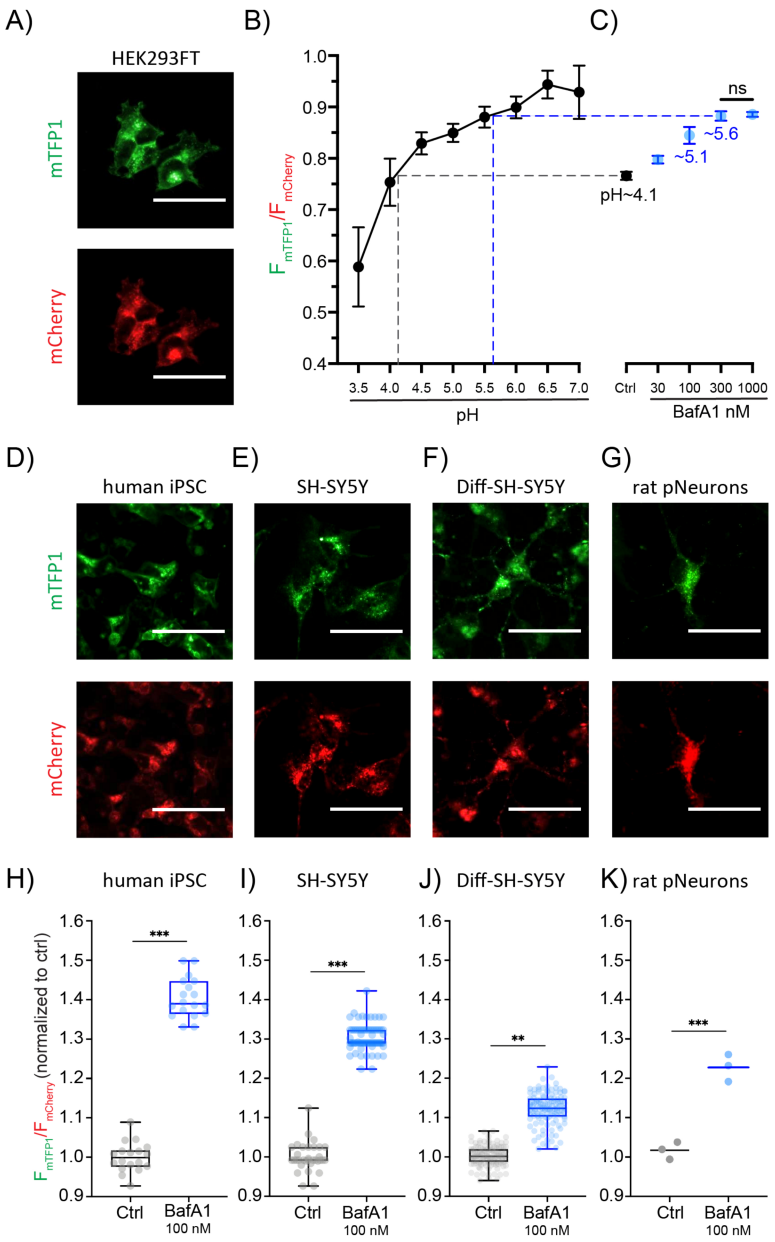

Figure 4. *In vitro* FIRE-pHLy models and relative pH measurements with bafilomycin A1

(A) Representative mTFP1 and mCherry ratiometric images of PFA-fixed FIRE-pHLy-expressing HEK293FT cells taken on a high-content confocal imaging system. Scale bars = 10 µm. **(B)** pH calibration curve generated from fixed, pH buffer (pH 3.5 – 7.0) treated cells. Data points are presented as mean ± S.D., from 4 independent replicates; n = 10,000 cells per replicate. **(C)** FIRE-pHLy fluorescence ratios ($F_{mTFP1}/F_{mCherry}$) of FIRE-pHLy-expressing HEK293FT cells treated with bafilomycin (BafA1 30 nM to 1000 nM) and 0.1% DMSO (control) for 6 hours. Data points are presented as mean ± S.D., from 6 independent replicates; n = 10,000 cells per replicate. Tukey's test for multiple stepwise comparisons indicated significance between all groups including control, except BafA1 300 nM and 1000 nM. **(D-G)** Ratiometric images (left to right) of FIRE-pHLy stably expressed in human

366 iPSCs, SH-SY5Y, Differentiated SH-SY5Y, and late embryonic rat hippocampal neuronal cells. All cells were fixed
367 prior to image acquisition. Scale bar = 50 μm. **(H-K)** 100 nM bafilomycin A1 was treated on cells for 6 hours and
368 compared to 0.1% DMSO solvent control. Box-and-whisker plots show median, interquartile range (25th-75th
369 percentile) and maximum/minimum values of mean ratios per well. **(H)** human iPSC; 18 independent replicates; n =
370 15,000 cells per replicate. **(I)** SH-SY5Y; 76 independent replicates; n = 1,000 cells per replicate. **(J)** RA-
371 differentiated SH-SY5Y; 120 independent replicates; n = 3,000 cells per replicate. **(K)** primary rat hippocampal
372 neurons; 3 independent replicates; n = 10,000 cells per replicate. Statistical analysis was performed using two-tailed,
373 unpaired Student's *t*-test. *$p \leq 0.05$; **$p \leq 0.01$; ***$p \leq 0.001$; ns = not significant.
374
375 These results were consistent with our previous observations that FIRE-pHLy
376 reproducibly and accurately detected lysosomal pH perturbation in cells, highlighting the
377 potential of mapping pH in a variety of cell types and conditions.
378
379 **Monitoring FIRE-pHLy functions *in vivo***
380 From *in vitro* experiments using live and fixed cells, we further validated FIRE-pHLy
381 using *in vivo* imaging. *C. elegans* has been a powerful model system for studying the basic
382 biology of aging, cell death and many other biological phenomena (Son et al., 2019; Z. Wang &
383 Sherwood, 2011). In addition, the nematode is highly amenable to genetic manipulation, has a
384 short lifespan, and can be easily imaged through its transparent body wall (Apfeld & Alper,
385 2018; Kao et al., 2011). In recent years, studies on lysosomal biology have taken advantage of
386 these features in *C. elegans* to determine key roles for the lysosome in stem cell maintenance
387 (Bohnert & Kenyon, 2017) and aging-associated phenomena (Sun et al., 2020). Thus, we adapted
388 FIRE-pHLy for study in *C. elegans.*

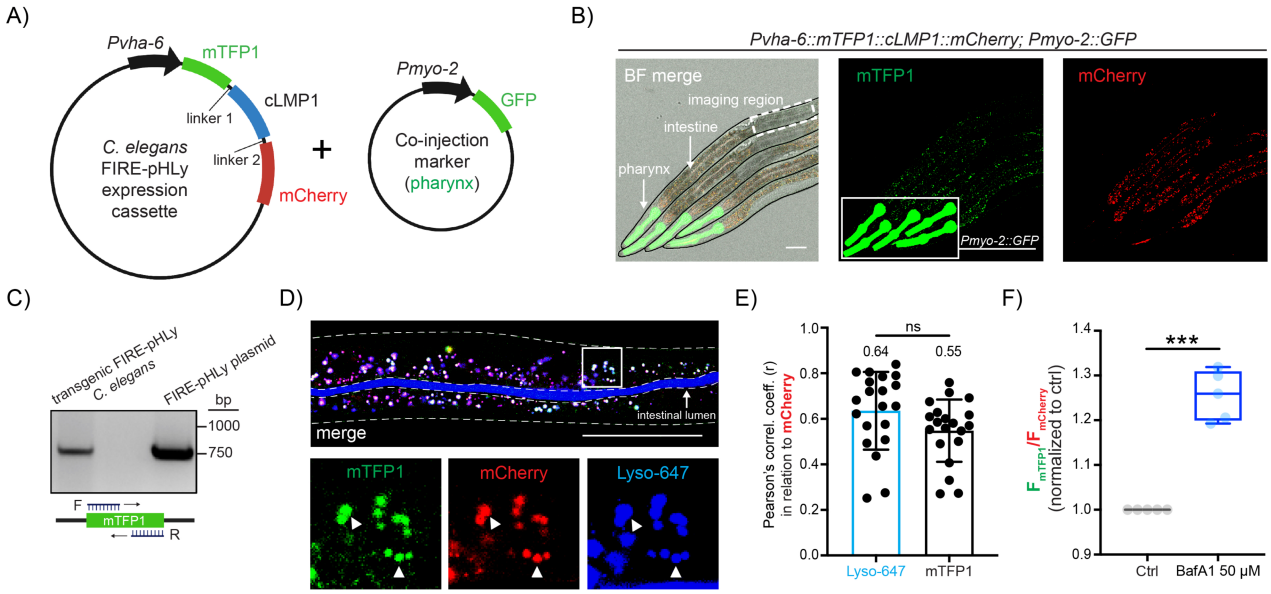

Figure 5: *In vivo* functional validation of FIRE-pHLy in *C. elegans*

(A) *C. elegans* FIRE-pHLy expression cassette driven by intestinal promoter *(*P*vha-6*::*mtfp1*::c*lmp1*::*mcherry)* co-injected with selection marker (P*myo-2*::*gfp*) expressed in the pharynx. The human LAMP1 sequence was exchanged for the *C. elegans* LAMP1 homolog, cLMP1. (**B**) Merged brightfield, mTFP1 and mCherry confocal images of 5 anaesthetized adult (L4) N2 worms expressing the FIRE-pHLy transgene and co-injection marker. Arrows indicate the pharynx and intestines. Dashed white box delineates a representative imaging region. Scale bar = 50 µm. **(C)** PCR sequencing of transgenic FIRE-pHLy-expressing worms and purified plasmid using forward & reverse mTFP1 specific primers. **(D)** Merged image showing Lyso-647 staining (shown in blue) with P*vha-6* driven expression of FIRE-pHLy expression (detected as punctuate structures) in intestinal tissue. White box shows zoomed insert of mTFP1, mCherry and Lyso-647 fluorescent puncta. Arrowheads highlight representative colocalized puncta. Scale bar = 50 µm. **(E)** Pearson's correlation coefficients (r) of Lyso-647 and mTFP1 colocalized with mCherry. Data points are presented as mean ± S.D., from n = 20 worms. Statistical analysis was performed using two-tailed, unpaired Student's *t*-test. **(F)** FIRE-pHLy fluorescence ratios ($F_{mTFP1}/F_{mCherry}$) of worm intestinal cells pre-incubated with 50 µM BafA1 and untreated control for 30 min. Box-and-whisker plot shows median, interquartile range (25th-75th percentile) and maximum/minimum values of mean ratios; 5 independent replicates; n = 18-20 worms/replicate. Statistical analysis was performed using two-tailed, unpaired Student's *t*-test. *$p \leq 0.05$; **$p \leq 0.01$; ***$p \leq 0.001$; ns = not significant.

Maintaining a similar topology, we generated an *in vivo* FIRE-pHLy expression vector by replacing the human LAMP1 signal peptide sequence with the homologous *C. elegans* cLMP1. The *vha-6* promoter was used to generate a nematode FIRE-pHLy with intestine-specific expression to allow ease of visualization and manipulation with BafA1 (**Fig. 5A**). *Pmyo-2::GFP* was utilized as a co-injection marker to allow for rapid selection of transgenic animals based on

412 bright pharyngeal expression **(Fig. 5B)**. Presence of the transgene was confirmed via polymerase
413 chain reaction **(Fig. 5C)**.
414 In live, anaesthetized, transgenic animals expressing FIRE-pHLy, mTFP1 and mCherry
415 fluorescence was detected on punctate structures morphologically similar to lysosomes that
416 colocalized with lysosomes marked with Lyso-647 (Pearson's coefficient value $r = 0.64 \pm 0.17$)
417 **(Fig. 5D-E)**. This confirmed trafficking and sorting of FIRE-pHLy to lysosomal compartments.
418 We also assessed FIRE-pHLy functionality by alkalinizing lysosomes in the intestines. Upon
419 BafA1 treatment, FIRE-pHLy ratios in transgenic *C. elegans* significantly increased in a
420 reproducible manner **(Fig. 5F)**. To summarize, we successfully demonstrated FIRE-pHLy
421 function *in vivo* in *C. elegans*, opening future avenues to profile lysosomal pH dynamics in a
422 tissue and age-specific manner.

423 **DISCUSSION**

424 Intracellular and intra-organellar pH, particularly that of lysosomes, plays a vital role in
425 regulating cellular homeostasis. Lysosomes are the key component in the degradation and
426 recycling of macromolecules, act as hubs for nutrient sensing and signaling, and are actively
427 involved with secretion and immune response (Settembre et al., 2013). Due to their ubiquitous
428 involvement in such fundamental processes, lysosomal dysfunction is linked to a host of
429 diseases. Lysosomes are biochemically defined by their low pH, which determines their
430 degradative capacity (Xu & Ren, 2015). Indeed, the proteolytic activity of lysosomes are
431 compromised in aging and age-related disorders (Martinez-Vicente et al., 2005), with evidence
432 supporting lysosomal acidification defects in neurodegenerative disorders such as Alzheimer's
433 disease (Wolfe et al., 2013). Additionally, dysregulated lysosomal pH is linked to tumorigenesis
434 (Glunde et al., 2003). Collectively, these findings have transformed our traditional understanding
435 of lysosomes as passive waste receptacles to dynamic participants in regulating cellular health
436 and disease, thus making them salient therapeutic targets (Appelqvist et al., 2013).

437 Given the central role of pH in lysosomal function and overall cellular homeostasis,
438 numerous lysosomal probes have been developed. Current technologies mostly include
439 fluorescent small molecules that rely on efficient uptake into cells (Han and Burgess, 2010;
440 Wolfe et al., 2013). As such, these probes are limited by their lack of lysosomal targeting
441 specificity, short-term imaging stability, cell-to-cell variability and inability to access all tissues
442 in multicellular organisms. Genetically encoded sensors, on the other hand, have the potential to
443 address these concerns, demonstrated for intracellular pH measurements (Benčina, 2013;
444 Gjetting et al., 2012; Grover et al., 2012; Martynov et al., 2018; Pakhomov et al., 2017;
445 Raimondo et al., 2013; Shirmanova et al., 2015; Tantama et al., 2011; Y. Zhang et al., 2012),
446 however, the field of lysosomal biology still lacks a robust genetically encoded pH biosensors.
447 For example, such sensors have already been widely explored in the field of calcium imaging
448 (M. Z. Lin & Schnitzer, 2016; Mank & Griesbeck, 2008). Therefore, we sought to engineer an
449 accessible genetically encoded detection tool to accurately and dynamically map pH under
450 different biological contexts. We generated genetically encoded FIRE-pHLy, a chimeric protein
451 biosensor **(Fig. 1)** that offered several technical and biological advantages compared to
452 previously described pH detection dyes. First, FIRE-pHLy was targeted very specifically to
453 lysosomal membranes with high degrees of colocalization with LAMP1 and LAMP2 **(Fig. 2)**.

454 This simultaneously addressed off-target subcellular localization issues and provided the ability
455 to accurately report pH in lysosomes, thus improving upon the precision of previous acidic
456 compartment probes.

457 Moreover, FIRE-pHLy can be easily expressed in a variety of model systems including
458 multiple cell types and organisms and thus overcome limitations of synthetic probes. Potentially,
459 FIRE-pHLy can be driven by different promoters to tune sensor levels in various cell types and
460 cell states, while minimizing overexpression artifacts. We generated stable FIRE-pHLy cell
461 models in HEK293FT, SH-SY5Y, differentiated SH-SY5Y, iPSC and primary rat neurons while
462 also targeting FIRE-pHLy expression to the intestinal tissue of *C. elegans* animals **(Fig. 4 and**
463 **5)**. FIRE-pHLy expression remained stable, which enables future comparisons of pH between
464 independent samples or experiments staged at longer time scales. This is important because
465 accurate and dynamic monitoring of lysosomal pH across time may uncover aging phenotypes
466 relevant to long-lived cells or animals. For example, lysosomal function and intracellular pH
467 dynamics can be explored in the context of cellular differentiation (in iPSCs or RA-differentiated
468 SH-SY5Y cells) or natural aging (in *C. elegans*) (Baxi et al., 2017; Chao et al., 2018; Lawrence
469 & Zoncu, 2019; Sun et al., 2020). To validate our models, bafilomycin treatment was used to
470 alkalinize lysosomes and confirmed a consistent increase in lysosomal pH (**Fig 4 and 5**).
471 Interestingly, we observed cell type differences in the extent of relative pH response. This
472 suggests context-dependent pH regulatory and compensatory mechanisms that warrant further
473 investigation.

474 Molecularly, mTFP1 offers a number of favorable attributes for a pH sensor because of
475 its titratable fluorescence within the physiological lysosomal pH range. mTFP1 has a pKa ~4.3,
476 signifying that only 50% of fluorescence molecules will be quenched at that value and lower pH
477 values may be recorded (Ai et al., 2006; Shinoda et al., 2018). Additionally, mTFP1 also resists
478 common FP pitfalls such as photobleaching and aggregation. Accordingly, FIRE-pHLy is tuned
479 to detect pH changes within the range of 3.0 to 6.0, which captures the physiological pH range of
480 lysosomes with 0.5-unit accuracy as demonstrated by unbiased high-content imaging and
481 quantification methods (**Fig. 3**).

482 We would like to acknowledge that recently, two related sensors containing mCherry-
483 pHluorin-LAMP1 (Ponsford et al., 2020) and sfGFP-LAMP1-mCherry fusions (Webb et al.,
484 2020) have been published. The described probes have a reported pKa of ~6.5 and ~5.0,

485 respectively. However, to our knowledge, FIRE-pHLy is the first lysosome-targeted pH
486 biosensor that incorporates mTFP1 as its novel pH-sensing domain with a pKa of 4.3 that
487 allowed for pH measurements within the extremely acidic range of physiological lysosomes.
488 FIRE-pHLy is also the first ratiometric lysosomal pH biosensor that was adapted to meet the
489 unique demands of both *in vitro* or *in vivo* systems. In the future, we hope to manipulate FIRE-
490 pHLy expression patterns using numerous *C. elegans* tissue specific promoters to elucidate
491 potential correlations between lysosomal pH and function in the context of development, aging
492 and in disease models. Moreover, by changing the targeting partner (i.e. LAMP1), mTFP1-
493 mediated pH measurements can be easily targeted to any specific subcellular compartments (e.g.
494 endosomes, mitochondria, endoplasmic reticulum, Golgi apparatus), thus making it a highly
495 versatile tool for measuring organelle-specific pH.

496 FIRE-pHLy can be easily imaged on most fluorescence microscopes because it is
497 amenable to ratiometric imaging on standard GFP (488 nm) and mCherry (561 nm) filter sets. In
498 addition to traditional live confocal microscopy, we also performed high-content imaging and
499 unbiased quantitative analyses using FIRE-pHLy on fixed cells. We found that FIRE-pHLy
500 fluorescence is not quenched during fixation, which enables high-throughput imaging
501 applications. FIRE-pHLy signal is bright and distinct, which allows for accurate feature
502 extraction of lysosomes in multiplexed quantitative workflows in cells. Thus, FIRE-pHLy could
503 be adapted to high-throughput screening platforms for drug discovery purposes.

504 During optimization of our pH calibration curve in live cells, we observed a decrease in
505 mCherry fluorescence associated with prolonged use of ionophores in extreme low pH (2.0 –
506 4.0). This ionophore-dependent quenching has been previously observed, and the general
507 recommendation is to limit exposure with ionophores by imaging the samples within 10 to 30
508 minutes after nigericin or monensin buffer addition (Canton & Grinstein, 2017; Grillo-Hill et al.,
509 2014; H.-J. Lin et al., 2003; Wolfe et al., 2013). This issue can be resolved by fixing the cells;
510 however, the calibration dynamic range becomes tighter **(Fig. 3 & 4).** Clearly, this problem
511 exists only with the artificial conditions required for ionophore calibrations and does not affect
512 whole-cell measurements of lysosomal lumenal pH under physiological conditions. Analysis of
513 individual mTFP1 and mCherry fluorescence intensity under bafilomycin treatment, which
514 selectively elevates lumenal pH of lysosomes but not cytosolic pH **(Supplementary Fig. 1A)**,
515 confirmed that only mTFP1 fluorescence varies with lysosomal pH change **(Supplementary Fig.**

516 **1B, C)**. Therefore, we recommend that ionophore concentration should be optimized separately
517 for each particular model before generating pH calibration curves.

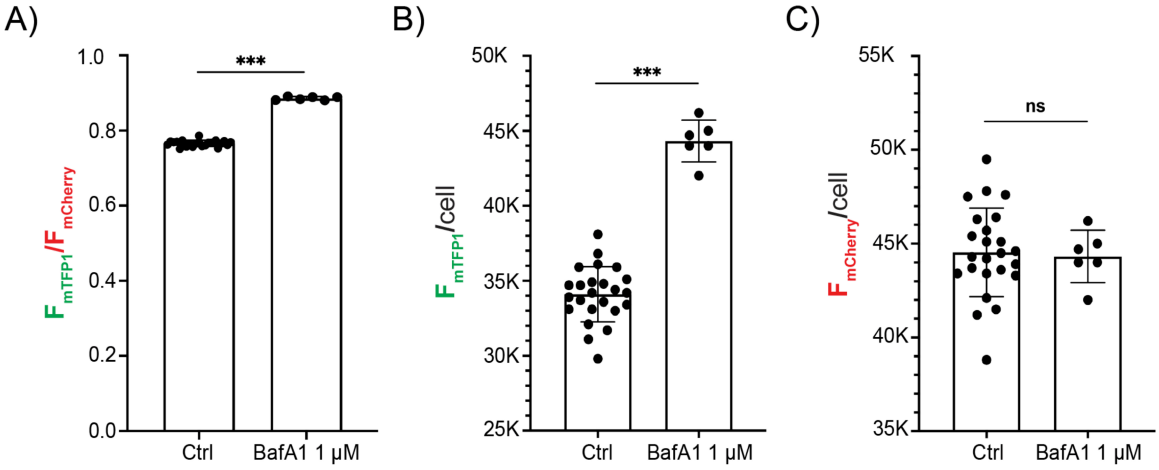

518 **Supplementary Figure 1: Ratiometric validation of individual FIRE-pHLy fluorophores**
519 (**A**) $F_{mTFP1}/F_{mCherry}$ ratio quantified from FIRE-pHLy-expressing HEK293FT cells treated with 1 μM bafilomycin for
520 6 hours compared to 0.1% DMSO solvent control. (**B**) mTFP1 mean fluorescence intensity normalized by cell count.
521 (**C**) mCherry mean fluorescence intensity normalized by cell count. Data points are presented as mean ± S.D., from
522 6 independent replicates; n=10,000 cells per replicate. Statistical analysis was performed using two-tailed, unpaired
523 Welch's *t*-test for unequal variances. *$p \leq 0.05$; **$p \leq 0.01$; ***$p \leq 0.001$; ns = not significant.
524

525 **CONCLUSION**

526 In summary, we have developed FIRE-pHLy, a novel genetically encoded ratiometric pH
527 biosensor that localizes to lysosomal membranes and measures lumenal pH within physiological
528 ranges. FIRE-pHLy responds robustly to pH changes and is amenable to stable integration to
529 multiple biological models, including cell lines and animals. Moreover, FIRE-pHLy is amenable
530 to both live- and fixed-cell assays, and both high-resolution confocal microscopy and
531 quantitative high-content imaging. We anticipate that FIRE-pHLy will be applied to elucidate pH
532 dynamics in basic lysosomal biology and disease. It may also be translated to phenotypic-
533 screening platforms for drug discovery. And finally, by engineering *in vivo* models such as *C.*
534 *elegans,* this study opens new avenues to profile lysosomal functions in age related-neurological
535 and other diseases.
536

537 **METHODS**

538 **Construction of Fluorescence Indicator REporting pH in Lysosomes (FIRE-pHLy)**

539 The genetically encoded FIRE-pHLy reporter cassette consists of the following coding segments,
540 from the N-terminus: CMV-human LAMP1 signal peptide (84bp) – mTFP1 – flexible linker 1
541 (GGSGGGSGSGGGSG) – human LAMP1 – rigid linker 2 (PAPAPAP) - mCherry. Source of
542 different elements are as follows: LAMP1 signal peptide and human LAMP1 were PCR
543 amplified from LAMP1-mGFP (Addgene Plasmid #34831, kind gift from the Mark Von Zastrov
544 lab, UCSF), mTFP1 amplified from mTFP1-pBAD (Addgene Plasmid #54553), mCherry
545 amplified from pcDNA3.1-mCherry (Addgene Plasmid #128744). The DNA segments were
546 PCR amplified (Phusion® High-Fidelity PCR Master Mix, NEB, UK, #M0531) and fused with
547 Gibson recombination cloning method (Gibson Assembly® Master Mix, NEB, UK, #E2611) in
548 pEGFP-N3 empty backbone. The linker sequences were incorporated into the primer sequences.
549 The FIRE-pHLy expression cassette was cloned into lentiviral vectors with CMV promoter
550 (pLJM1-EGFP; Addgene Plasmid #19319) and hUbC promoter (FUGW; Addgene Plasmid
551 #14883) by Epoch Life Science services (Sugar Land,Texas, USA). To generate the *C. elegans*
552 version of FIRE-pHLy, DNA segments encoding *C. elegans* LMP1, mTFP1 and mCherry were
553 PCR amplified and cloned into a P*vha-6* containing pDONR P4-P1R backbone (a kind gift from
554 Kevah Ashrafi lab, UCSF) by Gibson Assembly. The P*myo-2::GFP* injection marker was also a
555 kind gift from the Ashrafi lab, UCSF. All clones were verified by sequencing (Elim
556 Biopharmaceuticals, Inc., Hayward, CA, USA).

557 **Cell culture and lentiviral transduction**

558 All cells were cultured at 37°C with 5% CO_2 atmosphere and maintained under standard
559 procedures. HEK293FT cells (Thermo Fisher Scientific; Carlsbad, CA, USA, #R70007) were
560 cultured in Dulbecco's Modified Eagle medium (DMEM; Life Technologies, Carlsbad, CA,
561 USA, #11-995-073) with 10% heat-inactivated fetal bovine serum (FBS; Gemini Bio,
562 Sacramento, CA, USA, #GEMZR039) containing 1% penicillin and streptomycin (pen/strep)
563 (Gibco; Thermo Fisher Scientific, Inc., Waltham, MA, USA, #15140122) with 500 µg/mL G418
564 sulfate antibiotic (Thermo Fisher Scientific, #11811031). SH-SY5Y cells (American Type
565 Culture Collection; ATCC, Maryland, USA, #CRL-2266) were maintained in 1:1 Eagle's
566 Minimum Essential Medium (EMEM; ATCC, #30-2003) and F12 medium (Life Technologies;
567 Carlsbad, CA, USA, #11765062) with 10% FBS and 1% pen/strep. Cells were trypsinized with

568 0.05% Trysin-EDTA solution (Sigma, St. Louis, MO, USA, #T4049) during routine passaging.
569 Lentiviral packaging and titer assessments of FIRE-pHLy-lentivirus were performed by the
570 UCSF ViraCore facility. For lentivirus transduction, HEK293FT and SH-SY5Y cells were plated
571 in 6-well plates and cultured to ~70% confluence. Protocol was modified for iPSCs and primary
572 rat neurons (see below). Lentivirus infections were carried out in the presence of 10 µg/mL of
573 polybrene (Sigma, St. Louis, MO, USA, #S2667) in complete media. 48 hours post-transduction,
574 cells were selected with 1 µg/mL puromycin (Millipore; Carlsbad, CA, USA, #540411) to
575 generate stable transgene-expressing cell lines. Long-term transgene expression was maintained
576 by selecting for resistance to puromycin at a final concentration of 1 µg/mL. SH-SY5Y cells
577 were sorted for green and red positive fluorescence signal on a SH800S Cell Sorter (Sony
578 Biotechnology) at the UCSF Laboratory of Cell Analysis.

579 **Generation of FIRE-pHLy-expressing iPSCs**

580 The F11350 iPSC line was obtained from the laboratory of Celeste Karch at Washington
581 University School of Medicine (Karch et al., 2019). Cells were maintained in matrigel (Corning,
582 #354277) coated plates using mTSER media (StemCell Technologies, Vancouver, Canada,
583 #05850), which was replaced every day. During passaging, cells were lifted using Accutase
584 (ThermoFisher Scientific, #A1110501) and then replated in media supplemented with 10 µM
585 ROCK inhibitor (Y-27632, StemCell Technologies, #72304). For the transduction of the virus,
586 iPSCs were plated onto matrigel-coated 24-well plates at a density of 50,000 cells per well.
587 Serial dilutions of the UbC promoter FIRE-pHLy lentiviral vector were prepared in mTSER
588 media with 4 µg/ml polybrene (Sigma, #S2667) Lentivirus media was allowed to transduce cells
589 for 24 hours and then fresh media changes were performed every day until 80% confluence was
590 reached. Clonal populations of green/red fluorescence positive cells were manually selected and
591 transferred into separate wells for expansion.

592 **Isolation of primary rat neurons and FIRE-pHLy lentivirus transduction**

593 Wildtype SAS Sprague Dawley rats (Charles River Laboratories, Wilmington, MA, USA) and
594 isolation reagents were a kind gift from the Molofsky Lab (UCSF). Embryos staged at day 18
595 were dissected from one pregnant rat and immediately placed in chilled brain dissection buffer
596 (HBSS-Ca^{2+}/Mg^{2+}-free with 10 mM HEPES buffer, pH 7.3). Brains were removed from 5
597 individual embryos and hippocampi halves were isolated after removal of the meninges.
598 Hippocampi were digested with trypsin/EDTA solution and DNAase at 37°C incubation for 25

599 min. Quenching buffer (HI-OVO diluted 1:5 in HBSS-Ca^{2+}/Mg^{2+}-free, with 50% glucose,
600 ovomucoid, bovine serum albumin, and DNAase) was subsequently added to inhibit trypsin
601 digestion. Following centrifugation and buffer removal, culture medium I (DMEM-high glucose,
602 L-glutamine-sodium pyruvate free) supplemented with 10% fetal calf serum (FCS) (not heat
603 activated) was added to partially digested hippocampi. Cells were then manually dissociated and
604 plated in poly-D-lysine coated 96-well plates (Greiner Bio-One, Kremsmünster, Austria,
605 #655956) at a density of 15,000 cells per well. After 24 hours, media was replaced with culture
606 medium II (Neurobasal medium, 1% heat inactivated FCS, 2% B27 supplement, 1X Glutamax I,
607 1X MycoZap plus, and 15mM NaCl). At DIV 5 (5 days in vitro), 5 µM 5-Fluorouracil was added
608 to curb glial cell proliferation. At DIV 7, neurons were transduced with UbC-FIRE-pHLy
609 lentivirus for 24 hours. Half media changes were performed every two days until DIV 14.

610 **RA-differentiation of FIRE-pHLy SH-SY5Y neuroblastoma cells**

611 SH-SY5Y cells were seeded in collagen type I-coated µClear 96-well plates (Greiner Bio-One,
612 #655956) at a density of 10,000 cells/cm^2 24 hours before start of differentiation. Differentiation
613 media was composed of 10 µM of retinoic acid (RA) (Sigma, #R2625) in EMEM/F12 media
614 supplemented with 10% FBS and 1% P/S. After 6 days of RA treatment, cells were treated for 4
615 days with 50 ng/mL of brain-derived growth factor (BDNF) (Peprotech, Rocky Hill, NJ, USA,
616 #450-02B) in serum-depleted EMEM/F12 media supplemented with 1% pen/strep (Alquezar et
617 al., 2020; Encinas et al., 2000).

618 **Antibodies & reagents**

619 *Immunofluorescence.* AlexaFluor 647 mouse-anti-hLAMP1 (1:500, Biolegend, Carlsbad, CA,
620 USA; #328611), AlexaFluor 647 mouse-anti-hLAMP2 (1:500, Biolegend, Carlsbad, CA, USA;
621 #354311), mouse-anti-EEA1 (1:1000, BD Biosciences; Franklin Lakes, NJ, USA; #610457),
622 AlexaFluor 647 goat anti-mouse (1:500, Life Technologies; #A21206). *Western blot.* hLAMP1
623 (1:1000, DSHB, University of Iowa, USA, #2296838). *Reagents.* LysoTracker Deep Red™
624 (Life Technologies; #L12492), MitoTracker Deep Red FM (Invitrogen; Carlsbad, CA, USA,
625 #M22426), Monensin solution 1000X (Invitrogen; #501129057), Nigericin solution (Sigma
626 Aldrich, USA, #SML1779), paraformaldehyde (PFA) solution (Fisher Scientific; #50980494),
627 glycine (Sigma; #G7126), bovine serum albumin (BSA) (Fisher Scientific; #BP1605100), D-
628 PBS (Sigma; #D8662), Saponin (Sigma; #S7900).

629 **Western blotting**

630 Lysates from FIRE-pHLy-expressing HEK293FT cells were collected from 1X RIPA buffer
631 (Fisher Scientific, #89900) supplemented with a cocktail of phosphatase and protease inhibitors
632 (Roche, Basel, Switzerland, #4693116001). Sample protein concentrations were determined
633 using the Pierce™ BCA Protein Assay kit (Thermo Scientific, #PI23225). Samples were loaded
634 onto a Novex NuPAGE SDS-PAGE gel system with MOPS running buffer (Life Technologies,
635 #NP001). Proteins were transferred onto nitrocellulose membranes and blotted with indicated
636 antibodies. Imaging of band intensities were performed on a LI-COR Odyssey Infrared System
637 (LI-COR Biosciences, Lincoln, NE, USA).

638 **Immunofluorescence and colocalization analysis**

639 FIRE-pHLy-expressing HEK293FT cells were plated in TC-grade chamber slides (μ-Slide 8-
640 well chamber slide, Ibidi, Gräfelfing, Germany, #50305795) at a density of 30,000 cells per well
641 for 24 hours. For uptake of organelle markers, cells were incubated with 30 nM LysoTracker
642 Deep Red or 30 nM MitoTracker Deep Red FM along with 1:1000 Hoechst dye (10mg/mL
643 Hoescht 33342 solution, ThermoFisher, #H3570) in culture medium at 37°C/5% CO_2 for 10 min.
644 For immunofluorescence staining, cells were washed once with 1X D-PBS (with $MgCl_2$ and
645 $CaCl_2$) and fixed with 2% PFA for 15 min at room temperature (RT). Then, cells were washed
646 once with glycine, blocked for 2 min with 2% BSA/D-PBS, and permeabilized with 0.01%
647 saponin/2% BSA for 1 min at RT. Cells were incubated with primary antibodies for 1 hour at
648 RT, secondary antibodies for 1 hour at RT shielded from light, and washed twice. Cells were
649 imaged using an inverted confocal line-scanning microscope (DMi8 CS Bino, Leica
650 Microsystems Inc., Wetzlar, Germany) with a 63x/1.40 oil-immersion objective lens at
651 2048x2048 pixel resolution. Fluorescence images was acquired with sequential scanning
652 between frames on the LAS X SP8 Control Software system using preset channel settings (Blue
653 Ex/Em: 405 nm/410-464nm; Green Ex/Em: 470 nm/474-624nm; Red Ex/Em: 587 nm/592-646
654 nm; Far Red Ex/Em: 653 nm/658-775 nm). Randomly acquired imaging fields were processed
655 and the Pearson's correlation coefficients were calculated using ImageJ (NIH, Maryland, USA)
656 (Schneider et al., 2012) plugin JACoP (Just Another Co-localization Plugin).

657 **pH calibration buffers and standard curve**

658 pH calibration buffers and procedures were adapted from a previously described study with few
659 modifications (Wolfe et al., 2013). Buffer recipe is described below, composed of 5 mM NaCl,

660 115 mM KCl, and 1.3 mM $MgSO_4 \cdot 7H_2O$, 25 mM MES buffer with pH adjusted in the range 2.0
661 – 7.0. Freshly made buffers were supplemented with 10µM nigericin and 1X monensin.

Stock Conc.	5M NaCl	1M KCl	1M $MgSO_4 \cdot 7H_2O$	0.5M MES	6.7mM Nigericin	Monensin (1000X)	1N KOH/ 1N HCl *	Final volume
Volume	10 µl	1150 µl	13 µl	500 µl	15 µl	10 µl	*	10ml
Final Conc.	5 mM	115 mM	1.3 mM	25 mM	10 µM	1X		(H_2O)

662
663 ***pH values are adjusted using pH meter with appropriate acid/base. (conc., concentration)**
664 On day 1, FIRE-pHLy-expressing HEK293FT cells were seeded at a density of 10,000 cells/well
665 resuspended in 100 µl media in collagen type-1 coated, black-bottom 96-well plates (µClear,
666 Greiner Bio-One; #655956). Plates were left in the culture hood at room temperature for 45 min
667 to allow for even cell distribution before incubated at 37°C/5.0% CO_2 overnight. On day 2, cell
668 nuclei were stained with 1:1000 (vol/well) Hoechst dye (10 mg/mL Hoescht 33342 solution,
669 ThermoFisher, #H3570) diluted in cell culture media for 20 min at 37°C/5.0% CO_2. After one
670 wash with 50 µl of 1X D-PBS, 50 µl of each pH titration buffer supplemented with 10 µM
671 nigericin and 1X monensin were added to wells and incubated at 37°C/5.0% CO_2 for 10 min
672 (note: do not exceed). Plates were then immediately imaged live on the IN Cell Analyzer 6500
673 HS (General Electric Life Sciences/Cytiva, Marlborough, MA, USA) and processed (see *High-*
674 *content confocal microscopy, feature extraction and ratiometric image analysis).* Liquid
675 dispensing and aspiration were performed using an automatic multichannel pipette (Voyager II,
676 INTEGRA Biosciences Corp, Hudson, NH, USA; #4722).

677 **Bafilomycin treatment assay in cells**

678 Cells were seeded and cultured on 96-well plates prior to addition of 100 nM bafilomycin A1
679 (LC Laboratories, Woburn, MA #B-1080). After 6 hours, cells were fixed with 2% PFA at room
680 temperature (RT) for 15 min and washed once with 1X D-PBS. Cells were stained with 1X
681 Hoechst dye for 20 min at RT protected from light and washed once with 1X D-PBS. Plates were
682 imaged on the IN Cell Analyzer 6500 HS and processed (see *High-content confocal microscopy,*
683 *feature extraction and ratiometric image analysis).*

684 **High-content confocal microscopy, feature extraction and ratiometric image analysis**

685 Black 96-well assay plates (µClear® bottom, Greiner Bio-One; #655956) were imaged using a
686 fully automated laser-scanning confocal cell imaging system (IN Cell Analyzer 6500HS, GE
687 Life Sciences) with a NIKON 20X/0.75, Plan Apo, CFI/60 objective lens and preset excitation

688 lasers (Blue 405 nm; Green: 488 nm; Red: 561 nm). Laser and software autofocus settings were
689 applied to determine a single optimal focus position. The EDGE confocal setting was used to
690 increase image resolution and improve downstream visualization and segmentation of
691 lysosomes. Nine images were acquired per well and were distributed in a 3X3 equidistant grid
692 positioned in the well center. Wells were imaged sequentially in a vertical orientation. Image
693 stack files were analyzed on a high-content image analysis software (IN Cell Developer Toolbox
694 v1.9, GE Life Sciences). Target set segmentation and quantification measures were developed
695 for individual channels and applied onto all sample images. Cell nuclei were segmented using a
696 preset nucleus type segmentation module. The size of nuclear mask was adjusted according to
697 the cell type. Visual inspection of several reference fields across multiple wells confirmed
698 segmentation accuracy. Total number of segmented nuclei was quantified per well. To quantify
699 FIRE-pHLy fluorescence, mCherry was used as the reference channel for segmenting lysosomes.
700 mCherry fluorescence provided a robust representation of FIRE-pHLy localization for the
701 purposes of delineating lysosomal objects, compared to mTFP1 fluorescence, whose signal
702 varies with lysosomal pH. A preset vesicle segmentation module was applied on the 561nm
703 source images with acceptance criteria (Dens-levels>300), min/max granule size (1-10um),
704 scales = 2, sensitivity = 33, low background, and no shape constraints settings. These settings
705 created an object "mask" for lysosomes, which was directly applied to 488nm source images to
706 segment mTFP1 identically as mCherry. Mean fluorescence intensities of mCherry and mTFP1
707 channels were generated and the ratios calculated. All measures were outputted as a Microsoft
708 Excel file for further analysis.

709 ***Caenorhabditis elegans (C. elegans)* maintenance and generation of transgenics**

710 *C. elegans* hermaphrodites were maintained on nematode growth medium (NGM) agar plates
711 seeded with E. coli bacterial strain OP50 at 20°C as previously described (Brenner, 1974). To
712 generate *C. elegans* strains expressing FIRE-pHLy, P*vha-6::*FIRE-pHLy and *Pmyo-2::GFP*
713 were microinjected together into the gonads of N2 adult worms following the standard procedure
714 as described in WormBook (Eisenmann, 2005). Transgenic clones were verified by PCR
715 sequencing using forward & reverse mTFP1 specific primers using the standard protocol
716 described in the WormBook.
717
718

719 ***C. elegans* LysoTracker, bafilomycin treatment & quantification**

720 Bafilomycin A1 treatment protocol was adapted from a previously described method (Ji et al.,
721 2006). L4 worms were treated with 50 µM BafA1 (Invivogen, San Diego, CA, USA #88899-55-
722 2) for 30 minutes. Lysotracker treatment followed the same protocol but with 2 µM
723 LysoTracker™ Deep Red (Life Technologies; #L12492). Worms were mounted on a 2% agarose
724 pad on a microscope slide with 5 µl of 2 mM levamisole and imaged individually on a Leica
725 DMi8 inverted confocal microscope using a 40x (BafA1 treatment) or 63x (LysoTracker
726 treatment) oil objective (NA 1.40) at 1024x1024 pixel resolution. For ratiometric measurements,
727 the posterior end of the worm was imaged to avoid the co-injection marker. Images were
728 processed in ImageJ using a customized Macroscript. Briefly, mCherry and mTFP1 frames were
729 thresholded by Otsu threshold. A mask was created using the thresholded mCherry frame. Using
730 this mask, mCherry and mTFP1 values were extracted and plotted. Co-localization between
731 channels was conducted using the ImageJ JaCoP plug-in application. Non-intestinal regions and
732 the intestinal lumen (appeared as a solid thick line from LysoTracker signal) were excluded
733 during colocalization analysis. Only intestinal tissue peripheral to the lumen was selected for
734 Pearson's correlation coefficient analysis.

735 **Data presentation, statistical analysis, and illustrations**

736 All data were generated from randomly selected sample populations from at least three
737 independent experiments represented unless otherwise mentioned in corresponding figure
738 legends. Statistical data were either presented in box–and-whisker plots with median,
739 interquartile range, and maximum & minimum values or bar graphs with mean ± S.E.M.
740 Multiple comparisons between groups were analyzed by one-way ANOVA with Tukey's test and
741 statistical significance for two sets of data was determined by two-tailed, unpaired Student's t-
742 test. All data plots and statistical analyses were performed using GraphPad Prism 8 with no
743 samples excluded. Significant differences between experimental groups were indicated as
744 *P<0.05; **P<0.01; ***P<0.001; Only P <0.05 was considered as statistically significant. NS =
745 not significant. Pre-processing of data was organized in Microsoft Excel. Cartoon schematics
746 were created on Biorender.com. Figures were assembled on Adobe Illustrator.

747 **DATA AND REAGENT AVAILABILITY**

748 The authors declare that all relevant data supporting the findings of this study are available
749 within the paper (and its Supplementary information file). Any data or reagents can be obtained
750 from the corresponding authors (A.W.K. and M.R.A.) on reasonable request.

751 **ACKNOWLEDGEMENTS**

752 We greatly thank the Mark Von Zastrov lab (UCSF) for providing us with the hLAMP1-GFP
753 plasmid. We also thank Kevah Ashrafi lab for their generous gifts for the P*vha-6* containing
754 pDONR P4-P1R backbone, *Pmyo-2::GFP* injection marker and microinjection setup. We thank
755 Victoria Butler (Kao Lab) for training and assistance with microinjections and Mary Joanne de
756 Torres for worm maintenance. We are grateful for the guidance we received while working with
757 primary rat neurons at the Anna Molofsky lab (UCSF) and especially P. Nguyen for performing
758 the isolations and cell maintenance. We also acknowledge the UCSF Small Molecule Discovery
759 Center for their tremendous support and advice on our high-content imaging and analysis
760 protocols. Additionally, we thank members of the Kao and Arkin labs for their thoughtful
761 discussions. This work has received support from the NIH/NIA (R01 AG058447).

762 **AUTHOR CONTRIBUTIONS**

763 M.Y.C., A.R.P., M.G, M.R.A. and A.W.K for conceptualization and design; M.Y.C., A.R.P.,
764 K.A., A.L.W., C.A. and M.W. for experimental design and data acquisition; all authors analyzed
765 and interpreted data; M.Y.C., A.R.P., M.R.A. and A.W.K. wrote the manuscript; all authors
766 edited the manuscript.

767

768 **COMPETING INTERESTS STATEMENT**

769 The authors declare no competing financial interests.

REFERENCES

Ai, H., Henderson, J. N., Remington, S. J., & Campbell, R. E. (2006). Directed evolution of a monomeric, bright and photostable version of Clavularia cyan fluorescent protein: Structural characterization and applications in fluorescence imaging. *Biochemical Journal*, *400*(Pt 3), 531–540. https://doi.org/10.1042/BJ20060874

Alquezar, C., Felix, J. B., McCandlish, E., Buckley, B. T., Caparros-Lefebvre, D., Karch, C. M., Golbe, L. I., & Kao, A. W. (2020). Heavy metals contaminating the environment of a progressive supranuclear palsy cluster induce tau accumulation and cell death in cultured neurons. *Scientific Reports*, *10*. https://doi.org/10.1038/s41598-019-56930-w

Anderson, M., Moshnikova, A., Engelman, D. M., Reshetnyak, Y. K., & Andreev, O. A. (2016). Probe for the measurement of cell surface pH in vivo and ex vivo. *Proceedings of the National Academy of Sciences*, *113*(29), 8177–8181. https://doi.org/10.1073/pnas.1608247113

Apfeld, J., & Alper, S. (2018). What Can We Learn About Human Disease from the Nematode C. elegans? *Methods in Molecular Biology (Clifton, N.J.)*, *1706*, 53–75. https://doi.org/10.1007/978-1-4939-7471-9_4

Appelqvist, H., Wäster, P., Kågedal, K., & Öllinger, K. (2013). The lysosome: From waste bag to potential therapeutic target. *Journal of Molecular Cell Biology*, *5*(4), 214–226. https://doi.org/10.1093/jmcb/mjt022

Ashby, M. C., Ibaraki, K., & Henley, J. M. (2004). It's green outside: Tracking cell surface proteins with pH-sensitive GFP. *Trends in Neurosciences*, *27*(5), 257–261. https://doi.org/10.1016/j.tins.2004.03.010

Ballabio, A., & Bonifacino, J. S. (2020). Lysosomes as dynamic regulators of cell and organismal homeostasis. *Nature Reviews Molecular Cell Biology*, *21*(2), 101–118. https://doi.org/10.1038/s41580-019-0185-4

Baxi, K., Ghavidel, A., Waddell, B., Harkness, T. A., & Carvalho, C. E. de. (2017). Regulation of Lysosomal Function by the DAF-16 Forkhead Transcription Factor Couples Reproduction to Aging in Caenorhabditis elegans. *Genetics*, *207*(1), 83–101. https://doi.org/10.1534/genetics.117.204222

Benčina, M. (2013). Illumination of the Spatial Order of Intracellular pH by Genetically Encoded pH-Sensitive Sensors. *Sensors (Basel, Switzerland)*, *13*(12), 16736–16758. https://doi.org/10.3390/s131216736

Beyenbach, K. W., & Wieczorek, H. (2006). The V-type H+ ATPase: Molecular structure and function, physiological roles and regulation. *Journal of Experimental Biology*, *209*(4), 577–589. https://doi.org/10.1242/jeb.02014

Bohnert, K. A., & Kenyon, C. (2017). A lysosomal switch triggers proteostasis renewal in the immortal C. elegans germ lineage. *Nature*, *551*(7682), 629–633. https://doi.org/10.1038/nature24620

Bourdenx, M., Daniel, J., Genin, E., Soria, F. N., Blanchard-Desce, M., Bezard, E., & Dehay, B. (2016). Nanoparticles restore lysosomal acidification defects: Implications for Parkinson and other lysosomal-related diseases. *Autophagy*, *12*(3), 472–483. https://doi.org/10.1080/15548627.2015.1136769

Braulke, T., & Bonifacino, J. S. (2009). Sorting of lysosomal proteins. *Biochimica Et Biophysica Acta*, *1793*(4), 605–614. https://doi.org/10.1016/j.bbamcr.2008.10.016

Brenner, S. (1974). The Genetics of CAENORHABDITIS ELEGANS. *Genetics*, *77*(1), 71–94.

Brooks, A. R., Harkins, R. N., Wang, P., Qian, H. S., Liu, P., & Rubanyi, G. M. (2004). Transcriptional silencing is associated with extensive methylation of the CMV promoter following adenoviral gene delivery to muscle. *The Journal of Gene Medicine*, *6*(4), 395–404. https://doi.org/10.1002/jgm.516

Canton, J., & Grinstein, S. (2017). Measuring Phagosomal pH by Fluorescence Microscopy. In R. Botelho (Ed.), *Phagocytosis and Phagosomes: Methods and Protocols* (pp. 185–199). Springer. https://doi.org/10.1007/978-1-4939-6581-6_12

Casey, J. R., Grinstein, S., & Orlowski, J. (2010). Sensors and regulators of intracellular pH. *Nature Reviews Molecular Cell Biology*, *11*(1), 50–61. https://doi.org/10.1038/nrm2820

Chao, S.-C., Wu, G.-J., Huang, S.-F., Dai, N.-T., Huang, H.-K., Chou, M.-F., Tsai, Y.-T., Lee, S.-P., & Loh, S.-H. (2018). Functional and molecular mechanism of intracellular pH regulation in human inducible pluripotent stem cells. *World Journal of Stem Cells*, *10*(12), 196–211. https://doi.org/10.4252/wjsc.v10.i12.196

Chazotte, B. (2011). Labeling Lysosomes in Live Cells with LysoTracker. *Cold Spring Harbor Protocols*, *2011*(2), pdb.prot5571. https://doi.org/10.1101/pdb.prot5571

Chen, X., Zaro, J., & Shen, W.-C. (2013). Fusion Protein Linkers: Property, Design and Functionality. *Advanced Drug Delivery Reviews*, *65*(10), 1357–1369. https://doi.org/10.1016/j.addr.2012.09.039

Coffey, E. E., Beckel, J. M., Laties, A. M., & Mitchell, C. H. (2014). Lysosomal alkalization and dysfunction in human fibroblasts with the Alzheimer's disease-linked presenilin 1 A246E mutation can be reversed with cAMP. *Neuroscience*, *263*, 111–124. https://doi.org/10.1016/j.neuroscience.2014.01.001

Cranfill, P. J., Sell, B. R., Baird, M. A., Allen, J. R., Lavagnino, Z., de Gruiter, H. M., Kremers, G.-J., Davidson, M. W., Ustione, A., & Piston, D. W. (2016). Quantitative Assessment of Fluorescent Proteins. *Nature Methods*, *13*(7), 557–562. https://doi.org/10.1038/nmeth.3891

de Duve, C., & Wattiaux, R. (1966). Functions of Lysosomes. *Annual Review of Physiology*, *28*(1), 435–492. https://doi.org/10.1146/annurev.ph.28.030166.002251

Deus, C. M., Yambire, K. F., Oliveira, P. J., & Raimundo, N. (2020). Mitochondria–Lysosome Crosstalk: From Physiology to Neurodegeneration. *Trends in Molecular Medicine*, *26*(1), 71–88. https://doi.org/10.1016/j.molmed.2019.10.009

Dröse, S., & Altendorf, K. (1996). *BAFILOMYCINS AND CONCANAMYCINS AS INHIBITORS OF V-ATPases AND*. 8.

Eisenmann, D. M. (2005). Wnt signaling. *WormBook: The Online Review of C. Elegans Biology*, 1–17. https://doi.org/10.1895/wormbook.1.7.1

Encinas, M., Iglesias, M., Liu, Y., Wang, H., Muhaisen, A., Ceña, V., Gallego, C., & Comella, J. X. (2000). Sequential Treatment of SH-SY5Y Cells with Retinoic Acid and Brain-Derived Neurotrophic Factor Gives Rise to Fully Differentiated, Neurotrophic Factor-Dependent, Human Neuron-Like Cells. *Journal of Neurochemistry*, *75*(3), 991–1003. https://doi.org/10.1046/j.1471-4159.2000.0750991.x

Eskelinen, E.-L. (2006). Roles of LAMP-1 and LAMP-2 in lysosome biogenesis and autophagy. *Molecular Aspects of Medicine*, *27*(5), 495–502. https://doi.org/10.1016/j.mam.2006.08.005

Fang, B., Wang, D., Huang, M., Yu, G., & Li, H. (2010). Hypothesis on the Relationship Between the Change in Intracellular pH and Incidence of Sporadic Alzheimer's Disease or Vascular Dementia. *International Journal of Neuroscience*, *120*(9), 591–595. https://doi.org/10.3109/00207454.2010.505353

Gallagher, F. A., Kettunen, M. I., Day, S. E., Hu, D.-E., Ardenkjær-Larsen, J. H., Zandt, R. in 't, Jensen, P. R., Karlsson, M., Golman, K., Lerche, M. H., & Brindle, K. M. (2008). Magnetic resonance imaging of pH in vivo using hyperpolarized 13C-labelled bicarbonate. *Nature*, *453*(7197), 940–943. https://doi.org/10.1038/nature07017

Gjetting, K. S. K., Ytting, C. K., Schulz, A., & Fuglsang, A. T. (2012). Live imaging of intra- and extracellular pH in plants using pHusion, a novel genetically encoded biosensor. *Journal of Experimental Botany*, *63*(8), 3207–3218. https://doi.org/10.1093/jxb/ers040

Glunde, K., Guggino, S. E., Solaiyappan, M., Pathak, A. P., Ichikawa, Y., & Bhujwalla, Z. M. (2003). Extracellular Acidification Alters Lysosomal Trafficking in Human Breast Cancer Cells. *Neoplasia (New York, N.Y.)*, *5*(6), 533–545.

Grillo-Hill, B. K., Webb, B. A., & Barber, D. L. (2014). Ratiometric Imaging of pH Probes. In *Methods in Cell Biology* (Vol. 123, pp. 429–448). Elsevier. https://doi.org/10.1016/B978-0-12-420138-5.00023-9

Grover, A., Schmidt, B. F., Salter, R. D., Watkins, S. C., Waggoner, A. S., & Bruchez, M. P. (2012). A Genetically Encoded pH Sensor for Tracking Surface Proteins through Endocytosis**. *Angewandte Chemie (International Ed. in English)*, *51*(20), 4838–4842. https://doi.org/10.1002/anie.201108107

Han, J., & Burgess, K. (2010). Fluorescent Indicators for Intracellular pH. *Chemical Reviews*, *110*(5), 2709–2728. https://doi.org/10.1021/cr900249z

Harned, R. L., Hidy, P. H., Corum, C. J., & Jones, K. L. (1951). Nigericin a new crystalline antibiotic from an unidentified Streptomyces. *Antibiotics & Chemotherapy (Northfield, Ill.)*, *1*(9), 594–596.

Hughes, A. L., & Gottschling, D. E. (2012). An early age increase in vacuolar pH limits mitochondrial function and lifespan in yeast. *Nature*, *492*(7428), 261–265. https://doi.org/10.1038/nature11654

Huynh, K., Eskelinen El, Cc, S., A, M., P, S., & S, G. (2007). LAMP proteins are required for fusion of lysosomes with phagosomes. *The EMBO Journal*, *26*(2), 313–324. https://doi.org/10.1038/sj.emboj.7601511

Inoue, H., Noumi, T., Nagata, M., Murakami, H., & Kanazawa, H. (1999). Targeted disruption of the gene encoding the proteolipid subunit of mouse vacuolar H+-ATPase leads to early embryonic lethality. *Biochimica et Biophysica Acta (BBA) - Bioenergetics*, *1413*(3), 130–138. https://doi.org/10.1016/S0005-2728(99)00096-1

Ishida, Y., Nayak, S., Mindell, J. A., & Grabe, M. (2013). A model of lysosomal pH regulation. *The Journal of General Physiology*, *141*(6), 705–720. https://doi.org/10.1085/jgp.201210930

Jin, T., Sasaki, A., Kinjo, M., & Miyazaki, J. (2010). A quantum dot-based ratiometric pH sensor. *Chemical Communications*, *46*(14), 2408–2410. https://doi.org/10.1039/B921602B

Jovic, M., Sharma, M., Rahajeng, J., & Caplan, S. (2010). The early endosome: A busy sorting station for proteins at the crossroads. *Histology and Histopathology*, *25*(1), 99–112.

Kallunki, T., Olsen, O. D., & Jäättelä, M. (2013). Cancer-associated lysosomal changes: Friends or foes? *Oncogene*, *32*(16), 1995–2004. https://doi.org/10.1038/onc.2012.292

Kao, A. W., Rj, E., Lh, M., A, N., A, H., Ja, B., P, Z., A, de L., Lj, N., J, C., Jr, F. R., & C, K. (2011). A neurodegenerative disease mutation that accelerates the clearance of apoptotic cells. *Proceedings of the National Academy of Sciences of the United States of America*, *108*(11), 4441–4446. https://doi.org/10.1073/pnas.1100650108

Karch, C. M., Kao, A. W., Karydas, A., Onanuga, K., Martinez, R., Argouarch, A., Wang, C., Huang, C., Sohn, P. D., Bowles, K. R., Spina, S., Silva, M. C., Marsh, J. A., Hsu, S., Pugh, D. A., Ghoshal, N., Norton, J., Huang, Y., Lee, S. E., … Tau Consortium Stem Cell Group. (2019). A Comprehensive Resource for Induced Pluripotent Stem Cells from Patients with Primary Tauopathies. *Stem Cell Reports*, *13*(5), 939–955. https://doi.org/10.1016/j.stemcr.2019.09.006

Lahuerta, M., Aguado, C., Sánchez-Martín, P., Sanz, P., & Knecht, E. (2018). Degradation of altered mitochondria by autophagy is impaired in Lafora disease. *The FEBS Journal*, *285*(11), 2071–2090. https://doi.org/10.1111/febs.14468

Lambert, T. J. (2019). FPbase: A community-editable fluorescent protein database. *Nature Methods*, *16*(4), 277–278. https://doi.org/10.1038/s41592-019-0352-8

Lawrence, R. E., & Zoncu, R. (2019). The lysosome as a cellular centre for signalling, metabolism and quality control. *Nature Cell Biology*, *21*(2), 133–142. https://doi.org/10.1038/s41556-018-0244-7

Lee, J.-H., McBrayer, M. K., Wolfe, D. M., Haslett, L. J., Kumar, A., Sato, Y., Lie, P. P. Y., Mohan, P., Coffey, E. E., Kompella, U., Mitchell, C. H., Lloyd-Evans, E., & Nixon, R. A. (2015). Presenilin 1 Maintains Lysosomal Ca2+ Homeostasis via TRPML1 by Regulating vATPase-Mediated Lysosome Acidification. *Cell Reports*, *12*(9), 1430–1444. https://doi.org/10.1016/j.celrep.2015.07.050

Lin, H.-J., Herman, P., & Lakowicz, J. R. (2003). Fluorescence Lifetime-Resolved pH Imaging of Living Cells. *Cytometry. Part A : The Journal of the International Society for Analytical Cytology*, *52*(2), 77–89. https://doi.org/10.1002/cyto.a.10028

Lin, M. Z., & Schnitzer, M. J. (2016). Genetically encoded indicators of neuronal activity. *Nature Neuroscience*, *19*(9), 1142–1153. https://doi.org/10.1038/nn.4359

Liu, B., Palmfeldt, J., Lin, L., Colaço, A., Clemmensen, K. K. B., Huang, J., Xu, F., Liu, X., Maeda, K., Luo, Y., & Jäättelä, M. (2018). STAT3 associates with vacuolar H + -ATPase and regulates cytosolic and lysosomal pH. *Cell Research*, *28*(10), 996–1012. https://doi.org/10.1038/s41422-018-0080-0

Malik, B. R., Maddison, D. C., Smith, G. A., & Peters, O. M. (2019). Autophagic and endo-lysosomal dysfunction in neurodegenerative disease. *Molecular Brain*, *12*(1), 100. https://doi.org/10.1186/s13041-019-0504-x

Mank, M., & Griesbeck, O. (2008). Genetically encoded calcium indicators. *Chemical Reviews*, *108*(5), 1550–1564. https://doi.org/10.1021/cr078213v

Martinez-Vicente, M., Sovak, G., & Cuervo, A. M. (2005). Protein degradation and aging. *Experimental Gerontology*, *40*(8), 622–633. https://doi.org/10.1016/j.exger.2005.07.005

Martynov, V. I., Pakhomov, A. A., Deyev, I. E., & Petrenko, A. G. (2018). Genetically encoded fluorescent indicators for live cell pH imaging. *Biochimica et Biophysica Acta (BBA) - General Subjects*, *1862*(12), 2924–2939. https://doi.org/10.1016/j.bbagen.2018.09.013

Meilinger, D., Fellinger, K., Bultmann, S., Rothbauer, U., Bonapace, I. M., Klinkert, W. E. F., Spada, F., & Leonhardt, H. (2009). Np95 interacts with de novo DNA methyltransferases, Dnmt3a and Dnmt3b, and mediates epigenetic silencing of the viral CMV promoter in embryonic stem cells. *EMBO Reports*, *10*(11), 1259–1264. https://doi.org/10.1038/embor.2009.201

Miesenböck, G., De Angelis, D. A., & Rothman, J. E. (1998). Visualizing secretion and synaptic transmission with pH-sensitive green fluorescent proteins. *Nature*, *394*(6689), 192–195. https://doi.org/10.1038/28190

Mindell, J. A. (2012). Lysosomal Acidification Mechanisms. *Annual Review of Physiology*, *74*(1), 69–86. https://doi.org/10.1146/annurev-physiol-012110-142317

Mony, V. K., Benjamin, S., & O'Rourke, E. J. (2016). A lysosome-centered view of nutrient homeostasis. *Autophagy*, *12*(4), 619–631. https://doi.org/10.1080/15548627.2016.1147671

Mu, F.-T., Callaghan, J. M., Steele-Mortimer, O., Stenmark, H., Parton, R. G., Campbell, P. L., McCluskey, J., Yeo, J.-P., Tock, E. P. C., & Toh, B.-H. (1995). EEA1, an Early Endosome-Associated Protein. EEA1 IS A CONSERVED α-HELICAL PERIPHERAL MEMBRANE PROTEIN FLANKED BY CYSTEINE "FINGERS" AND CONTAINS A CALMODULIN-BINDING IQ MOTIF. *Journal of Biological Chemistry*, *270*(22), 13503–13511. https://doi.org/10.1074/jbc.270.22.13503

O'Connor, N., & Silver, R. B. (2013). Ratio Imaging. In *Methods in Cell Biology* (Vol. 114, pp. 387–406). Elsevier. https://doi.org/10.1016/B978-0-12-407761-4.00016-6

Ohkuma, S. (1989). Use of fluorescein isothiocyanate-dextran to measure proton pumping in lysosomes and related organelles. In *Methods in Enzymology* (Vol. 174, pp. 131–154). Elsevier. https://doi.org/10.1016/0076-6879(89)74015-5

Pakhomov, A. A., Martynov, V. I., Orsa, A. N., Bondarenko, A. A., Chertkova, R. V., Lukyanov, K. A., Petrenko, A. G., & Deyev, I. E. (2017). Fluorescent protein Dendra2 as a ratiometric genetically encoded pH-sensor.

Biochemical and Biophysical Research Communications, *493*(4), 1518–1521. https://doi.org/10.1016/j.bbrc.2017.09.170

Pierzyńska-Mach, A., Janowski, P. A., & Dobrucki, J. W. (2014). Evaluation of acridine orange, LysoTracker Red, and quinacrine as fluorescent probes for long-term tracking of acidic vesicles. *Cytometry Part A*, *85*(8), 729–737. https://doi.org/10.1002/cyto.a.22495

Platt, F. M., Boland, B., & van der Spoel, A. C. (2012). Lysosomal storage disorders: The cellular impact of lysosomal dysfunction. *The Journal of Cell Biology*, *199*(5), 723–734. https://doi.org/10.1083/jcb.201208152

Ponsford, A. H., Ryan, T. A., Raimondi, A., Cocucci, E., Wycislo, S. A., Fröhlich, F., Swan, L. E., & Stagi, M. (2020). Live imaging of intra-lysosome pH in cell lines and primary neuronal culture using a novel genetically encoded biosensor. *Autophagy*, 1–19. https://doi.org/10.1080/15548627.2020.1771858

Raimondo, J. V., Joyce, B., Kay, L., Schlagheck, T., Newey, S. E., Srinivas, S., & Akerman, C. J. (2013). A genetically-encoded chloride and pH sensor for dissociating ion dynamics in the nervous system. *Frontiers in Cellular Neuroscience*, *7*. https://doi.org/10.3389/fncel.2013.00202

Rodriguez, E. A., Campbell, R. E., Lin, J. Y., Lin, M. Z., Miyawaki, A., Palmer, A. E., Shu, X., Zhang, J., & Tsien, R. Y. (2017). The growing and glowing toolbox of fluorescent and photoactive proteins. *Trends in Biochemical Sciences*, *42*(2), 111–129. https://doi.org/10.1016/j.tibs.2016.09.010

Rohrer, J., Schweizer, A., Russell, D., & Kornfeld, S. (1996). The targeting of Lamp1 to lysosomes is dependent on the spacing of its cytoplasmic tail tyrosine sorting motif relative to the membrane. *The Journal of Cell Biology*, *132*(4), 565–576.

Rousseau, A., & Bertolotti, A. (2018). Regulation of proteasome assembly and activity in health and disease. *Nature Reviews Molecular Cell Biology*, *19*(11), 697–712. https://doi.org/10.1038/s41580-018-0040-z

Rudnick, G. (1987). The Vacuolar ATPase Is Responsible for Acidifying Secretory Organelles. *Annals of the New York Academy of Sciences*, *493*(1 Cellular and), 259–263. https://doi.org/10.1111/j.1749-6632.1987.tb27206.x

Saftig, P., & Klumperman, J. (2009). Lysosome biogenesis and lysosomal membrane proteins: Trafficking meets function. *Nature Reviews Molecular Cell Biology*, *10*(9), 623–635. https://doi.org/10.1038/nrm2745

Schneider, C. A., Rasband, W. S., & Eliceiri, K. W. (2012). NIH Image to ImageJ: 25 years of Image Analysis. *Nature Methods*, *9*(7), 671–675.

Settembre, C., Fraldi, A., Medina, D. L., & Ballabio, A. (2013). Signals for the lysosome: A control center for cellular clearance and energy metabolism. *Nature Reviews. Molecular Cell Biology*, *14*(5), 283–296. https://doi.org/10.1038/nrm3565

Shaner, N. C., Campbell, R. E., Steinbach, P. A., Giepmans, B. N. G., Palmer, A. E., & Tsien, R. Y. (2004). Improved monomeric red, orange and yellow fluorescent proteins derived from Discosoma sp. Red fluorescent protein. *Nature Biotechnology*, *22*(12), 1567–1572. https://doi.org/10.1038/nbt1037

Shcherbo, D., Merzlyak, E. M., Chepurnykh, T. V., Fradkov, A. F., Ermakova, G. V., Solovieva, E. A., Lukyanov, K. A., Bogdanova, E. A., Zaraisky, A. G., Lukyanov, S., & Chudakov, D. M. (2007). Bright far-red fluorescent protein for whole-body imaging. *Nature Methods*, *4*(9), 741–746. https://doi.org/10.1038/nmeth1083

Shemiakina, I. I., Ermakova, G. V., Cranfill, P. J., Baird, M. A., Evans, R. A., Souslova, E. A., Staroverov, D. B., Gorokhovatsky, A. Y., Putintseva, E. V., Gorodnicheva, T. V., Chepurnykh, T. V., Strukova, L., Lukyanov, S., Zaraisky, A. G., Davidson, M. W., Chudakov, D. M., & Shcherbo, D. (2012). A monomeric red fluorescent protein with low cytotoxicity. *Nature Communications*, *3*(1), 1204. https://doi.org/10.1038/ncomms2208

Shinoda, H., Shannon, M., & Nagai, T. (2018). Fluorescent Proteins for Investigating Biological Events in Acidic Environments. *International Journal of Molecular Sciences*, *19*(6). https://doi.org/10.3390/ijms19061548

Shirmanova, M. V., Druzhkova, I. N., Lukina, M. M., Matlashov, M. E., Belousov, V. V., Snopova, L. B., Prodanetz, N. N., Dudenkova, V. V., Lukyanov, S. A., & Zagaynova, E. V. (2015). Intracellular pH imaging in cancer cells in vitro and tumors in vivo using the new genetically encoded sensor SypHer2. *Biochimica et Biophysica Acta (BBA) - General Subjects*, *1850*(9), 1905–1911. https://doi.org/10.1016/j.bbagen.2015.05.001

Son, H. G., Altintas, O., Kim, E. J. E., Kwon, S., & Lee, S. V. (2019). Age-dependent changes and biomarkers of aging in Caenorhabditis elegans. *Aging Cell*, *18*(2). https://doi.org/10.1111/acel.12853

Sun, Y., Li, M., Zhao, D., Li, X., Yang, C., & Wang, X. (2020). Lysosome activity is modulated by multiple longevity pathways and is important for lifespan extension in C. elegans. *ELife*, *9*, e55745. https://doi.org/10.7554/eLife.55745

993 Tantama, M., Hung, Y. P., & Yellen, G. (2011). Imaging Intracellular pH in Live Cells with a Genetically-Encoded
994 Red Fluorescent Protein Sensor. *Journal of the American Chemical Society*, *133*(26), 10034–10037.
995 https://doi.org/10.1021/ja202902d
996 Tekirdag, K., & Cuervo, A. M. (2018). Chaperone-mediated autophagy and endosomal microautophagy: Jointed by
997 a chaperone. *The Journal of Biological Chemistry*, *293*(15), 5414–5424.
998 https://doi.org/10.1074/jbc.R117.818237
999 Van Acker, Z. P., Bretou, M., & Annaert, W. (2019). Endo-lysosomal dysregulations and late-onset Alzheimer's
1000 disease: Impact of genetic risk factors. *Molecular Neurodegeneration*, *14*. https://doi.org/10.1186/s13024-
1001 019-0323-7
1002 Wang, X., Fan, L., Wang, Y., Zhang, C., Liang, W., Shuang, S., & Dong, C. (2020). Visual monitoring of the
1003 lysosomal pH changes during autophagy with a red-emission fluorescent probe. *Journal of Materials*
1004 *Chemistry B*, *8*(7), 1466–1471. https://doi.org/10.1039/C9TB02551K
1005 Wang, Z., & Sherwood, D. R. (2011). Dissection of Genetic Pathways in C. elegans. *Methods in Cell Biology*, *106*,
1006 113–157. https://doi.org/10.1016/B978-0-12-544172-8.00005-0
1007 Webb, B. A., Chimenti, M., Jacobson, M. P., & Barber, D. L. (2011). Dysregulated pH: A perfect storm for cancer
1008 progression. *Nature Reviews Cancer*, *11*(9), 671–677. https://doi.org/10.1038/nrc3110
1009 Wilson, J. M., de Hoop, M., Zorzi, N., Toh, B.-H., Dotti, C. G., & Parton, R. G. (2000). EEA1, a Tethering Protein
1010 of the Early Sorting Endosome, Shows a Polarized Distribution in Hippocampal Neurons, Epithelial Cells,
1011 and Fibroblasts. *Molecular Biology of the Cell*, *11*(8), 2657–2671.
1012 Wolfe, D. M., Lee, J., Kumar, A., Lee, S., Orenstein, S. J., & Nixon, R. A. (2013). Autophagy failure in Alzheimer's
1013 disease and the role of defective lysosomal acidification. *The European Journal of Neuroscience*, *37*(12),
1014 1949–1961. https://doi.org/10.1111/ejn.12169
1015 Xu, H., & Ren, D. (2015). Lysosomal Physiology. *Annual Review of Physiology*, *77*, 57–80.
1016 https://doi.org/10.1146/annurev-physiol-021014-071649
1017 Zhang, X.-X., Wang, Z., Yue, X., Ma, Y., Kiesewetter, D. O., & Chen, X. (2013). pH-Sensitive Fluorescent Dyes:
1018 Are They Really pH-Sensitive in Cells? *Molecular Pharmaceutics*, *10*(5), 1910–1917.
1019 https://doi.org/10.1021/mp3006903
1020 Zhang, Y., Xie, Q., Robertson, J. B., & Johnson, C. H. (2012). pHlash: A New Genetically Encoded and Ratiometric
1021 Luminescence Sensor of Intracellular pH. *PLoS ONE*, *7*(8). https://doi.org/10.1371/journal.pone.0043072
1022
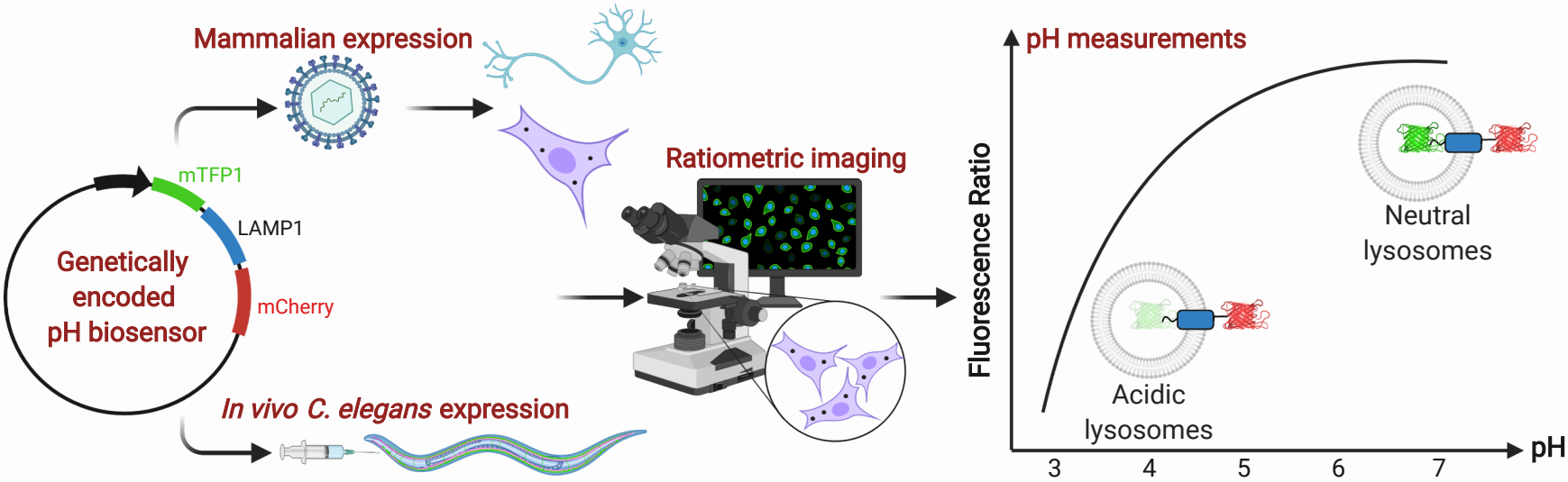
For Table of Contents Only